Facile Synthesis of stable, water soluble, dendron-coated gold nanoparticles

Alan E. Enciso, Giovanni Doni, Riccardo Nifosi, Ferruccio Palazzesi, Roberto Gonzalez, Ashley A. Ellsworth, Jeffrey L. Coffer, Amy V. Walker, Giovanni M. Pavan, Ahmed Mohamed, & Eric E. Simanek

Table of Contents

Contributions: AM conceived the experiments and supervised elements of execution. AEB executed the synthetic chemistry under the direction of EES (TCU). GD, RN, FP developed the computational strategies for the system under the direction of GMP (SUPSI). RG collected TEM images under the direction of JLC (TCU). AAE collected XPS and SIMS data under the direction of AVW (UT Dallas), who should be contacted for questions concerning these efforts.

General Experimental

Three different generation triazine dendrons (G0, G1, G2) were synthesized by known methods[a]. Each one of the dendrons was reacted overnight with a THF solution of 4-(aminomethyl)aniline. Afterwards the purification was accomplished by column chromatography.

The dendrons containing aniline were reacted with $H[AuCl_4]•3H_2O$ and $[NO]PF_6$ in acetonitrile in order to generate the diazonium moieties; the product was recovered by precipitation with diethyl ether. The corresponding diazonium salt was reduced with a solution 0.1M of $NaBH_4$ to form the grafted gold nanoparticles that were recovered by either filtration or centrifugation. All the species where analyzed under UV-vis, NMR, TEM besides of verifying the formation of the diazonium salts by IR.

[a] Enciso, A. E.; Abid, Z. M.; Simanek, E. E. *Polym. Chem*., **2014**, 5, 4635.

G0-aniline dendron

G0-Triazine Dendron (0.400 g, 0.532 mmol) was added to a solution of 4-(aminomethyl)aniline (0.325 g, 2.6 mmol) in THF (4 mL). Afterwards the solution was heated while stirring for 16 hours at 75ºC in a capped vessel. The crude product was purified by column chromatography. The solvent system used was the following: 100% DCM to 95:5 DCM: MeOH to give G0-aniline (0.347 g, 83%) as a yellowish oil. ^{1}H NMR (400 MHz, $CDCl_3$) δ 7.04-7.03 (dd, J = 7.6 Hz, 2H, m-aniline), 6.58-6.56 (dd, J = 8.3 Hz, 2H, o-aniline), 4.38 (br, 2H, aniline-C**H**$_2$-NH-triazine) 3.73-3.39 (m, 28H, C**H**$_2$OC**H**$_2$C**H**$_2$OC**H**$_2$C**H**$_2$OC**H**$_2$, C_3N_3-NHC**H**$_2$$CH_2CH_2O$), 3.17 (br m, 4H, BocNHC**H**$_2$), 1.77-1.68 (m, 8H, OCH_2C**H**$_2$$CH_2$), 1.44 (s, 18H, C(C**H**$_3$)$_3$); ^{13}C NMR (100 MHz, $CDCl_3$) δ 165.9 (**C**$_3$N$_3$), 156.1 (**C**O), 145.6 (H_2N-**C**(aniline)), 129.1 (p-aniline), 128.7 (m-aniline), 115.0 (o-aniline), 78.7 (**C**$(CH_3)_3$), 70.5 (O**C**H_2**C**H_2O), 70.2 (O**C**H_2**C**H_2O), 70.1 (O**C**H_2**C**H_2O), 69.4 (CH_2CH_2**C**H_2O), 69.2 (CH_2CH_2**C**H_2O), 44.1 (aniline-**C**H_2-NH-triazine), 38.4 (**C**$H_2CH_2CH_2O$), 38.1 (**C**$H_2CH_2CH_2O$) 29.6 (NHCH_2**C**H_2CH_2O), 29.5 (NHCH_2**C**H_2CH_2O), 28.4 (C(**C**H_3)$_3$); MS (ESI-TOF) calcd for $C_{40}H_{71}N_9O_{10}$ 837.53, found 838.54.

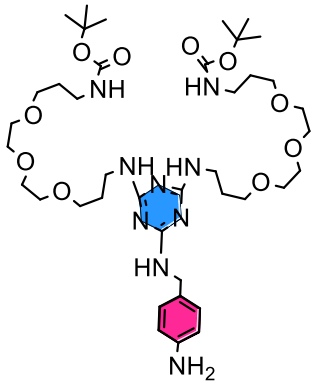

SI Figure 1 - ^{1}H NMR of G0 - Aniline Dendron

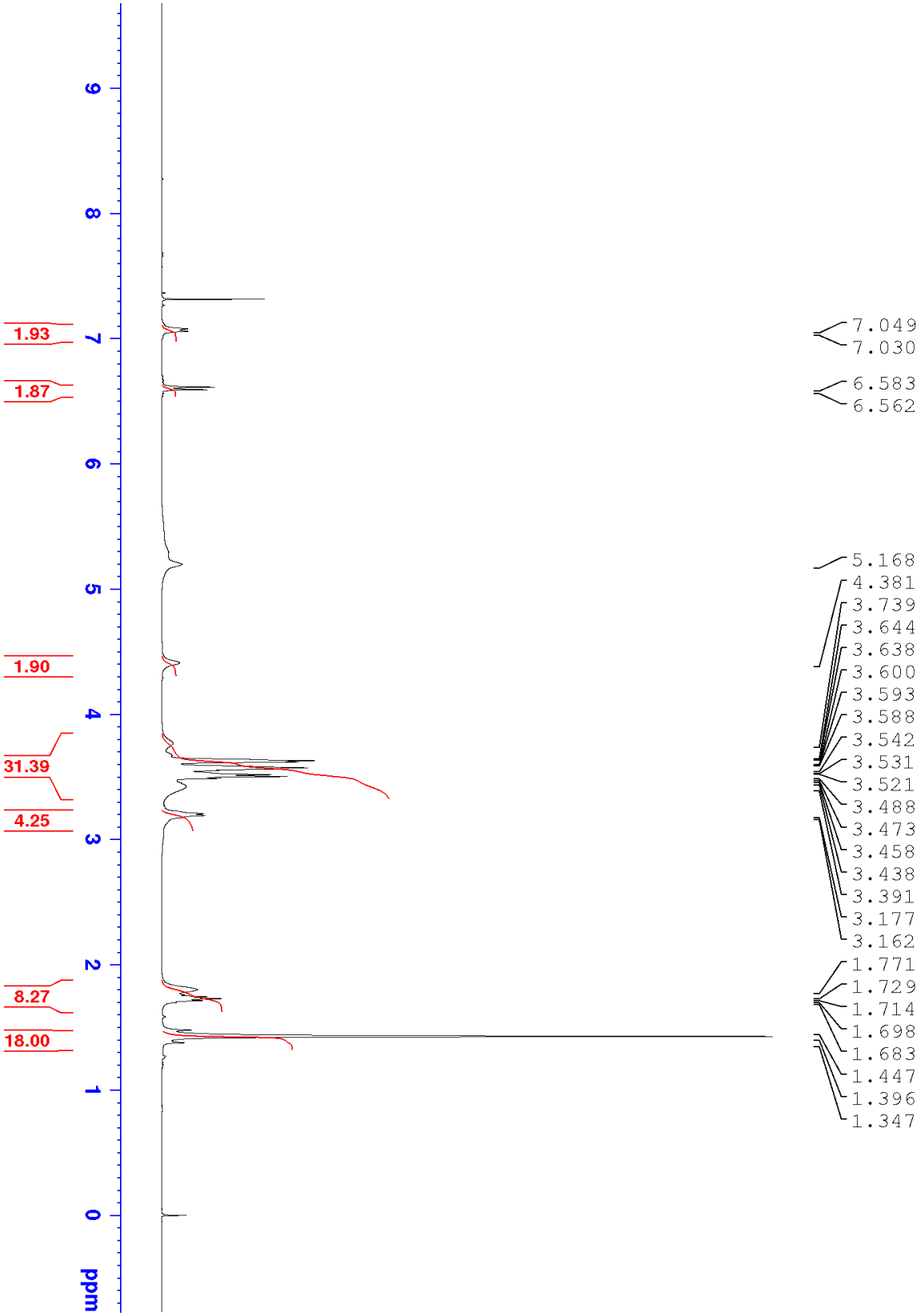

SI Figure 2- ^{13}C NMR of G0 - Aniline Dendron

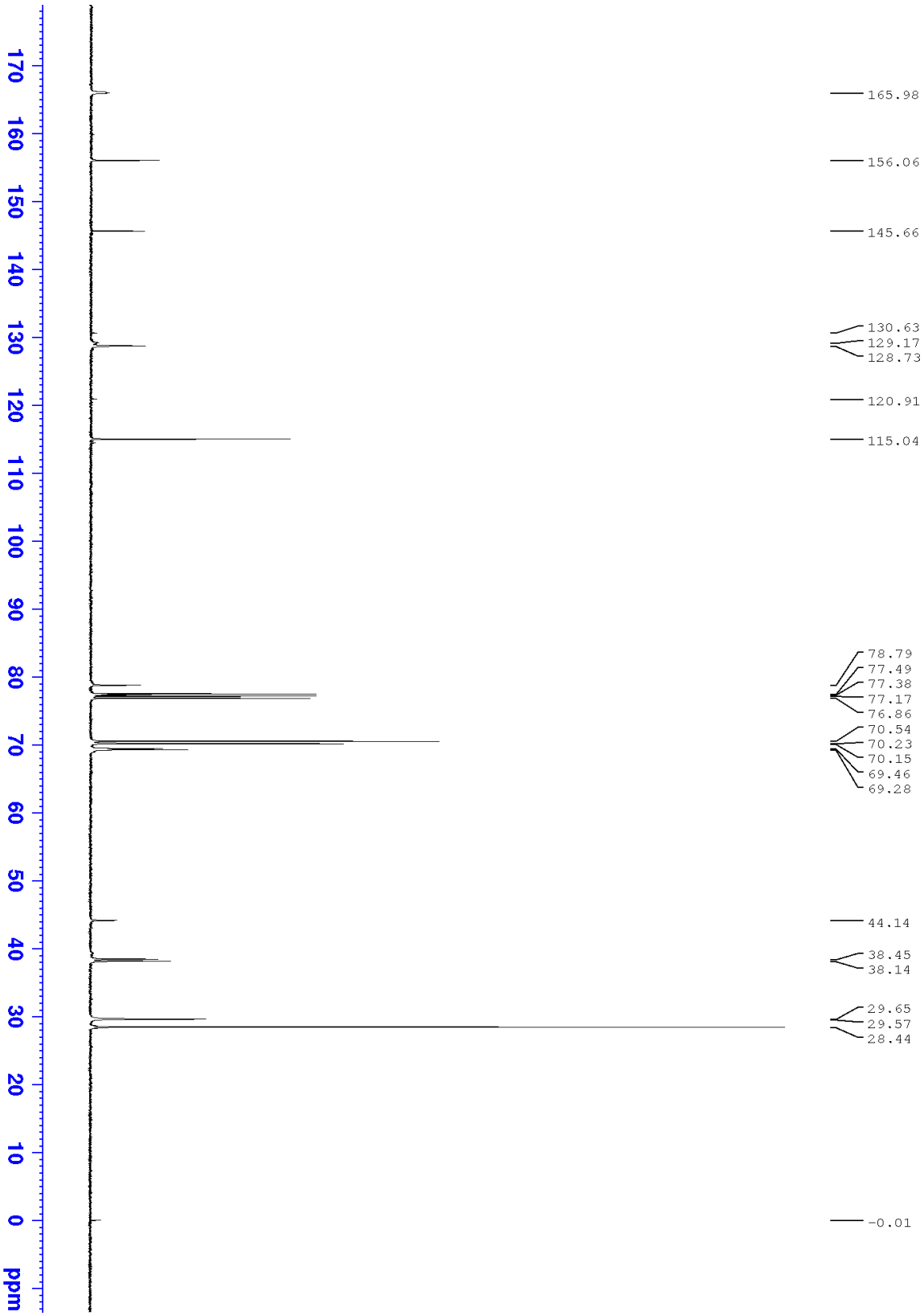

SI Figure 3 - Mass Spectra of G0- Aniline Dendron

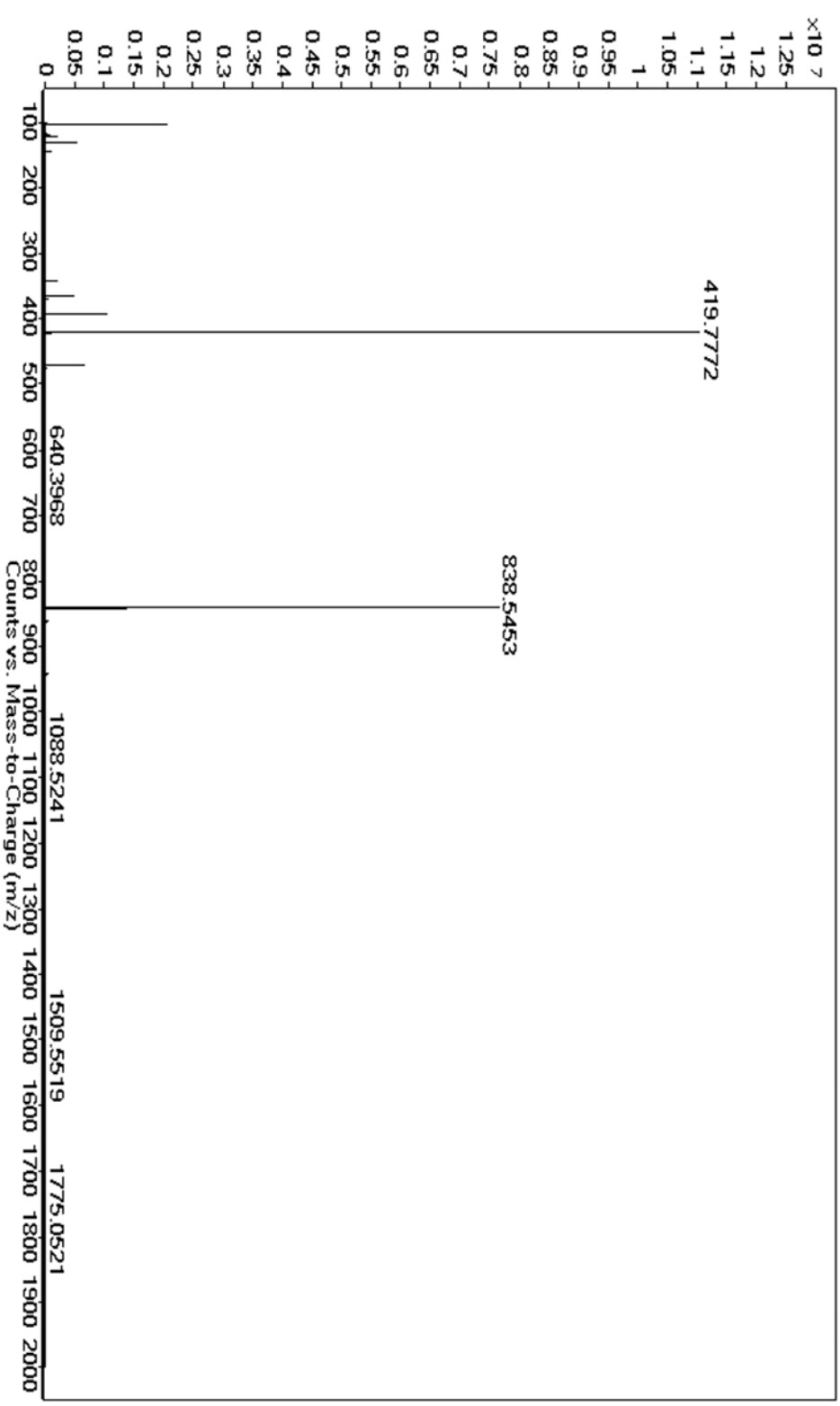

G1-aniline

G1-Triazine Dendron (0.400 g, 0.202 mmol) was added to a solution of 4-(aminomethyl)aniline (0.123 g, 1 mmol) in THF (2 mL). Afterwards the solution was heated while stirring for 16 hours at 75ºC in a capped vessel. The crude product was purified by column chromatography. The solvent system used was the following: 100% DCM to 90:10 DCM: MeOH to give G1-aniline (0.347 g, 83%) as a yellowish oil. ^{1}H NMR (400 MHz, $CDCl_3$) δ 7.07-7.05 (dd, J = 7.7 Hz, 2H, m-aniline), 6.60-6.58 (dd, J = 8.3 Hz, 2H, o-aniline), 4.40 (br, 2H, aniline-C**H**$_2$-NH-triazine) 3.63-3.39 (m, 88H, C**H**$_2$OC**H**$_2$C**H**$_2$OC**H**$_2$C**H**$_2$OC**H**$_2$, C_3N_3-NHC**H**$_2$$CH_2CH_2O$), 3.20 (br m, 8H, BocNHC**H**$_2$), 1.78-1.71 (m, 24H, OCH_2C**H**$_2$$CH_2$), 1.45 (s, 36H, C(C**H**$_3$)$_3$); ^{13}C NMR (100 MHz, $CDCl_3$) δ 166.0 (**C**$_3$N$_3$), 156.0 (**C**O), 145.6 (H_2N-**C**(aniline)), 129.1 (p-aniline), 128.7 (m-aniline), 115.0 (o-aniline), 78.8 (**C**$(CH_3)_3$), 70.5 (O**C**H_2**C**H_2O), 70.2 (O**C**H_2**C**H_2O), 70.1 (O**C**H_2**C**H_2O), 69.5 (CH_2CH_2**C**H_2O), 69.2 (CH_2CH_2**C**H_2O), 44.1 (aniline-**C**H_2-NH-triazine), 38.5 (**C**$H_2CH_2CH_2O$), 38.0 (**C**$H_2CH_2CH_2O$), 29.6 (two lines, $NHCH_2$**C**H_2CH_2O), 28.4 (C(**C**$H_3)_3$); MS (ESI-TOF) calcd for $C_{96}H_{177}N_{23}O_{26}$, 2068.32; found 2070.33.

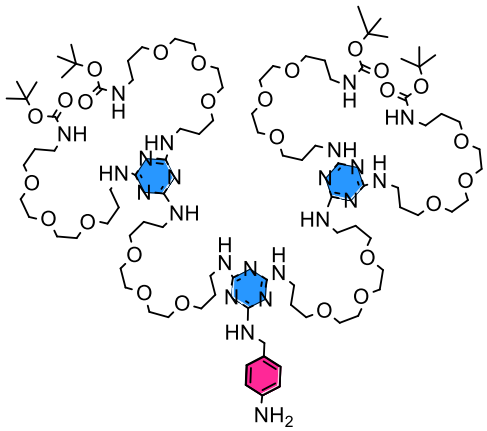

SI Figure 4 - ^{1}H NMR of G1- Aniline Dendron

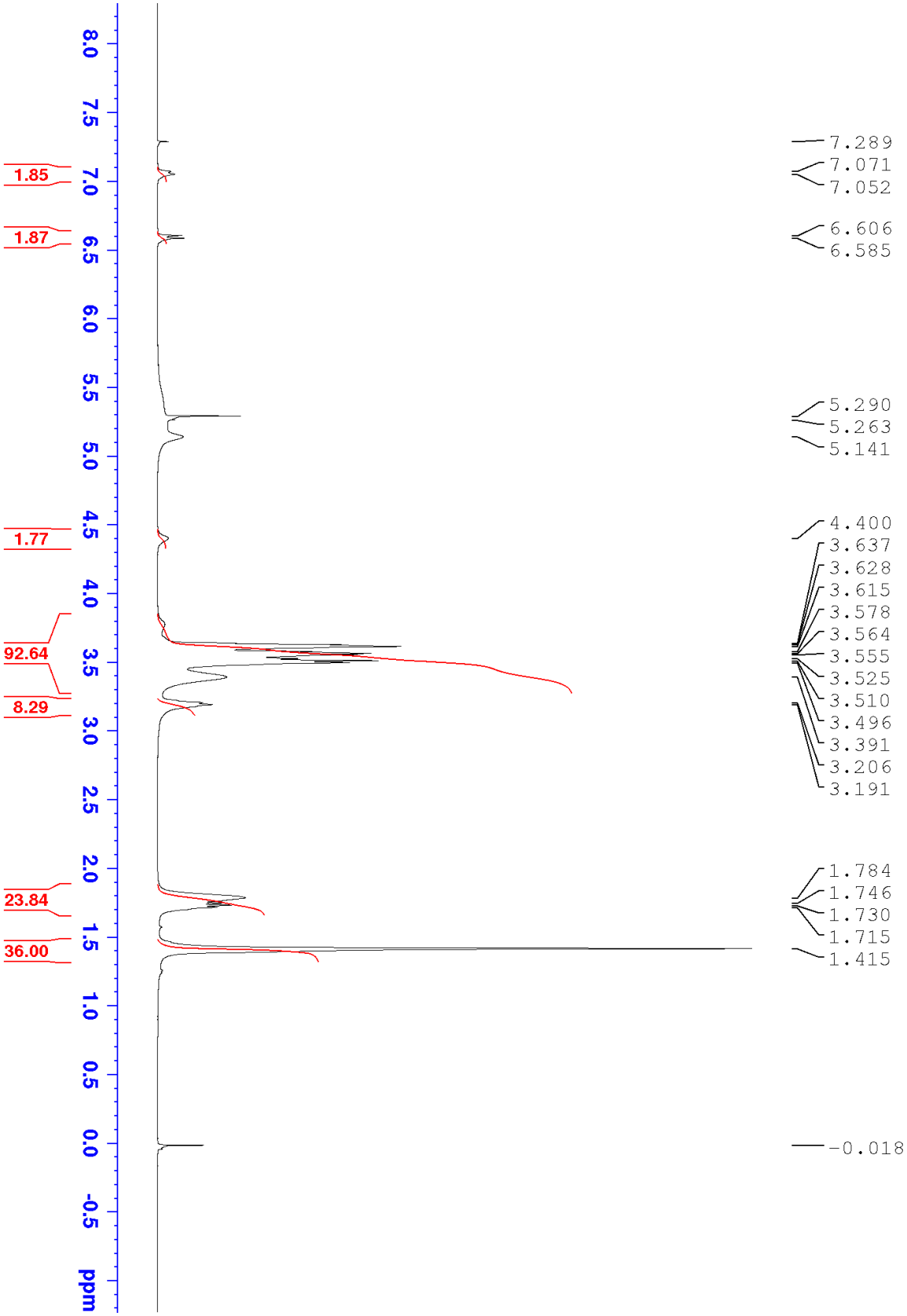

SI Figure 5 - ^{13}C NMR of G1- Aniline Dendron

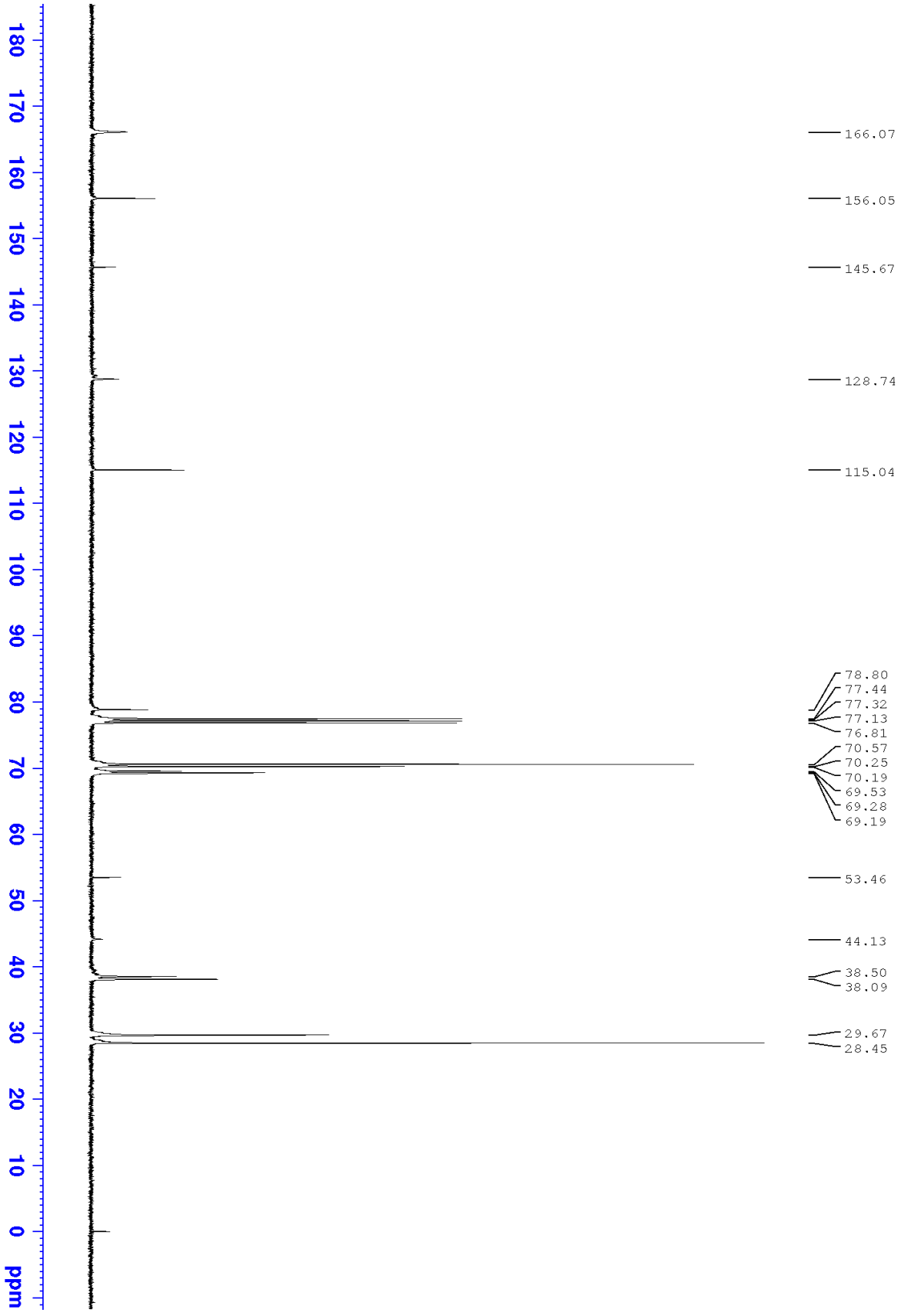

SI Figure 6 - Mass Spectra of G1- Aniline Dendron

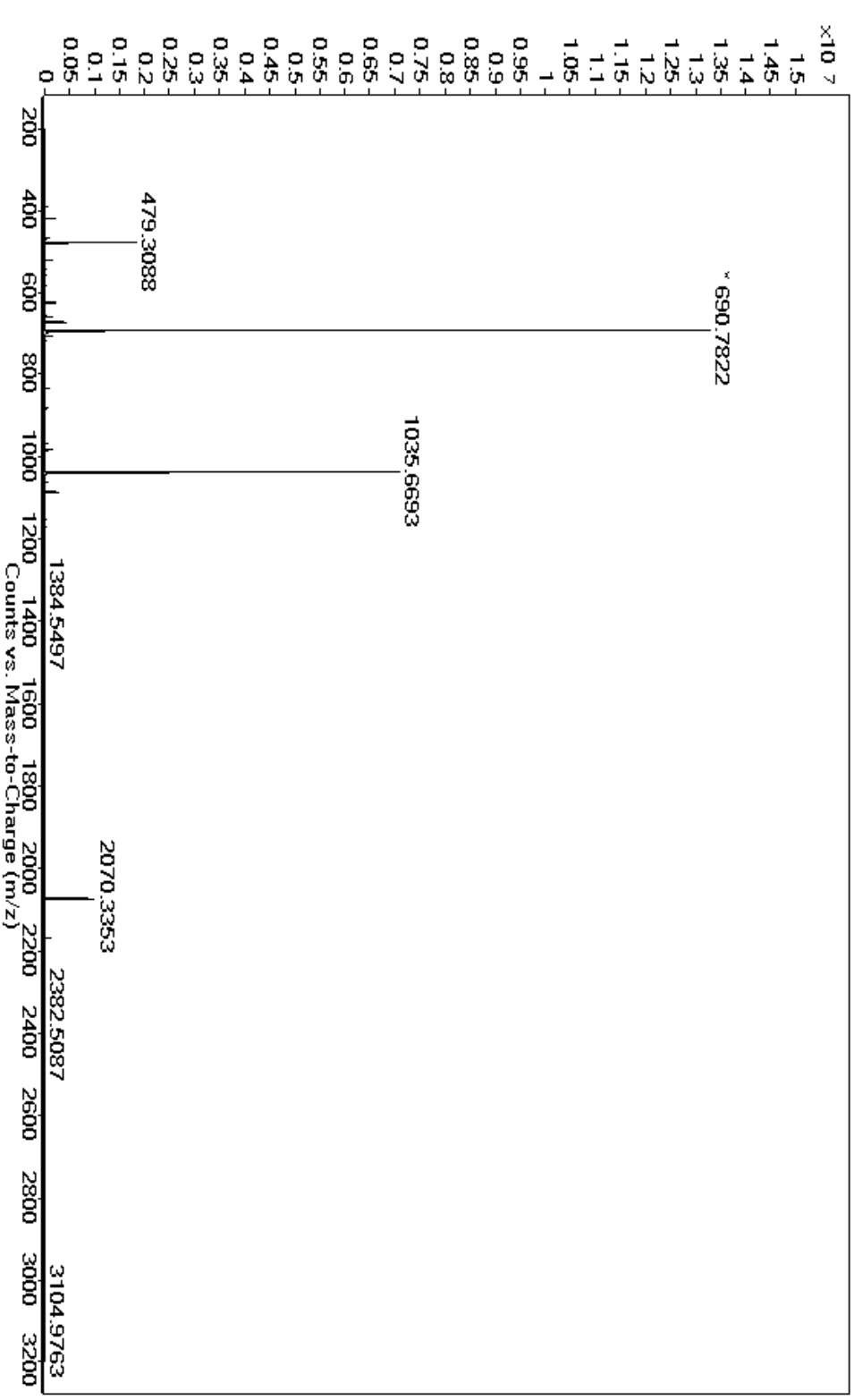

G2-aniline

G2-Triazine Dendron (0.400 g, 0.089 mmol) was added to a solution of 4-(aminomethyl)aniline (0.055 g, 0.450 mmol) in THF (2 mL). Afterwards the solution was heated while stirring for 16 hours at 75ºC in a capped vessel. The crude product was purified by column chromatography. The solvent system used was the following: 100% DCM to 90:10 DCM: MeOH to give G2-aniline (0.327 g, 80%) as a yellowish oil. ^{1}H NMR (400 MHz, $CDCl_3$) δ 7.02-7.00 (dd, J = 7.6 Hz, 2H, m-aniline), 6.56-6.54 (dd, J = 8.3 Hz, 2H, o-aniline), 4.36 (br, 2H, aniline-C**H**$_2$-NH-triazine) 3.69-3.36 (m, 208H, C**H**$_2$OC**H**$_2$C**H**$_2$OC**H**$_2$C**H**$_2$OC**H**$_2$, C_3N_3-NHC**H**$_2$$CH_2CH_2O$), 3.16 (br m, 16H, BocNHC**H**$_2$), 1.76-1.68 (m, 56H, OCH_2C**H**$_2$$CH_2$), 1.38 (s, 72H, C(C**H**$_3$)$_3$); ^{13}C NMR (100 MHz, $CDCl_3$) δ 165.8 (**C**$_3$N$_3$), 156.0 (**C**O), 145.7 (H_2N-**C**(aniline)), 129.1 (not found, p-aniline), 128.7 (m-aniline), 115.0 (o-aniline), 78.7 (**C**$(CH_3)_3$), 70.5 (OCH_2**C**H_2CH_2O), 70.2 (OCH_2**C**H_2CH_2O), 70.1 (two lines, O**C**H_2**C**H_2O), 69.4 (CH_2CH_2**C**H_2O), 69.2 (two lines, CH_2CH_2**C**H_2O), 44.1 (aniline-**C**H_2-NH-triazine), 38.4 (**C**$H_2CH_2CH_2O$), 38.0 (two lines, **C**$H_2CH_2CH_2O$), 29.6 (two lines, $NHCH_2$**C**H_2CH_2O), 28.4 (C(**C**$H_3)_3$); MS (ESI-TOF) calcd for $C_{208}H_{389}N_{51}O_{58}$, 4529.90; found 4531.96.

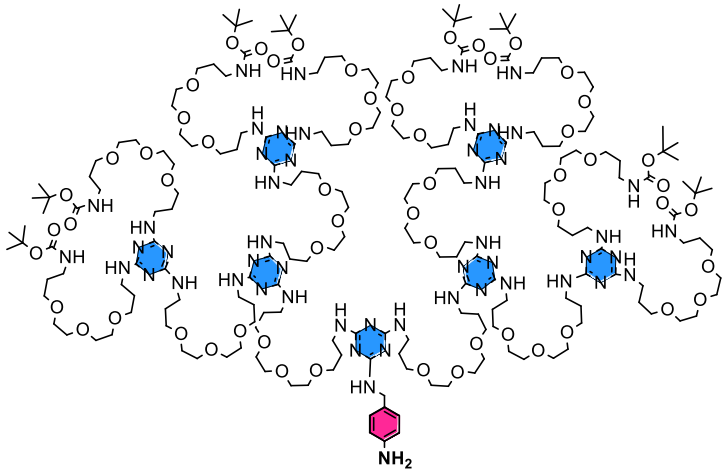

SI Figure 7 - ^{1}H NMR of G2 Aniline Dendron

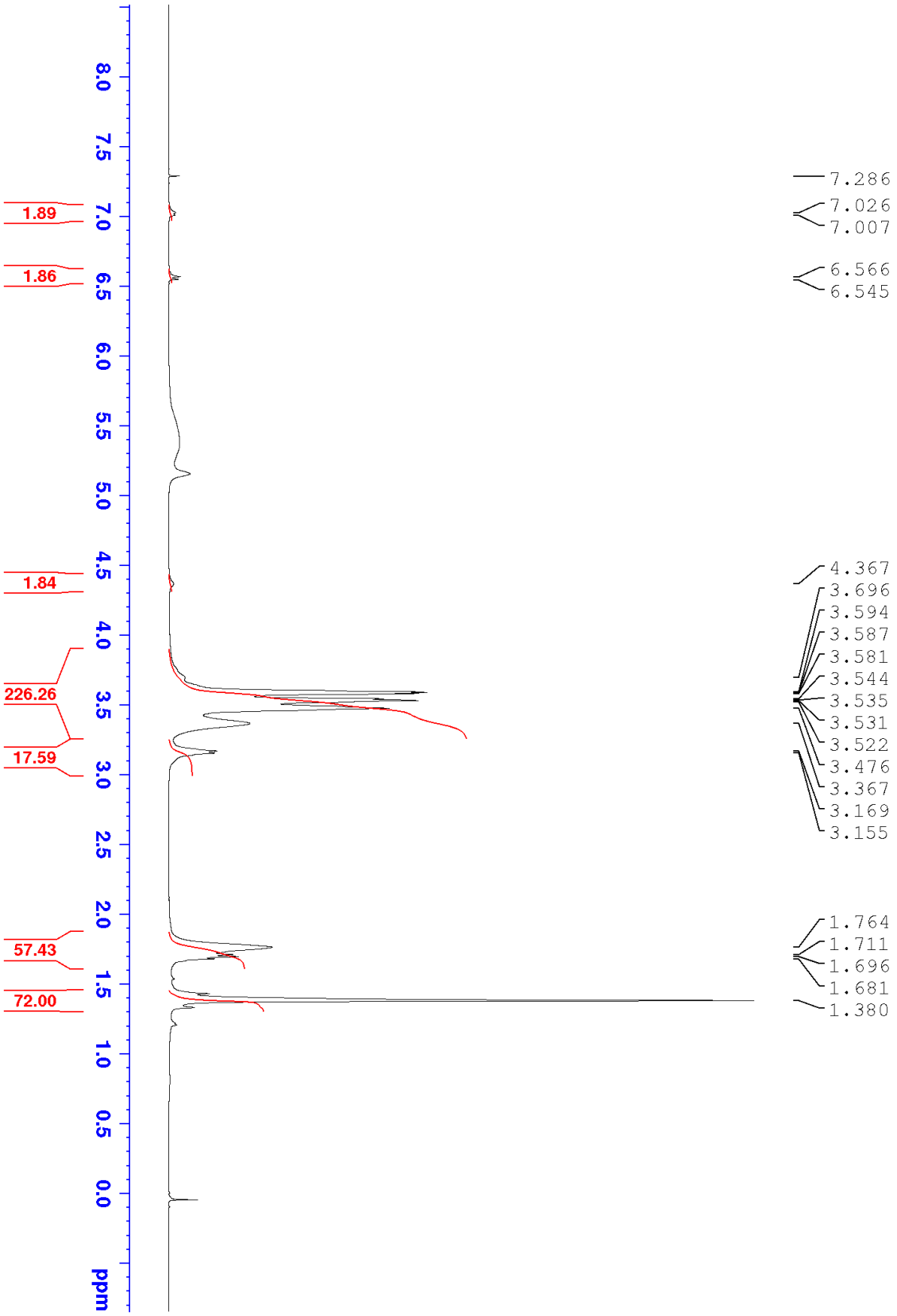

SI Figure 8 - ^{13}C NMR of G2 Aniline Dendron

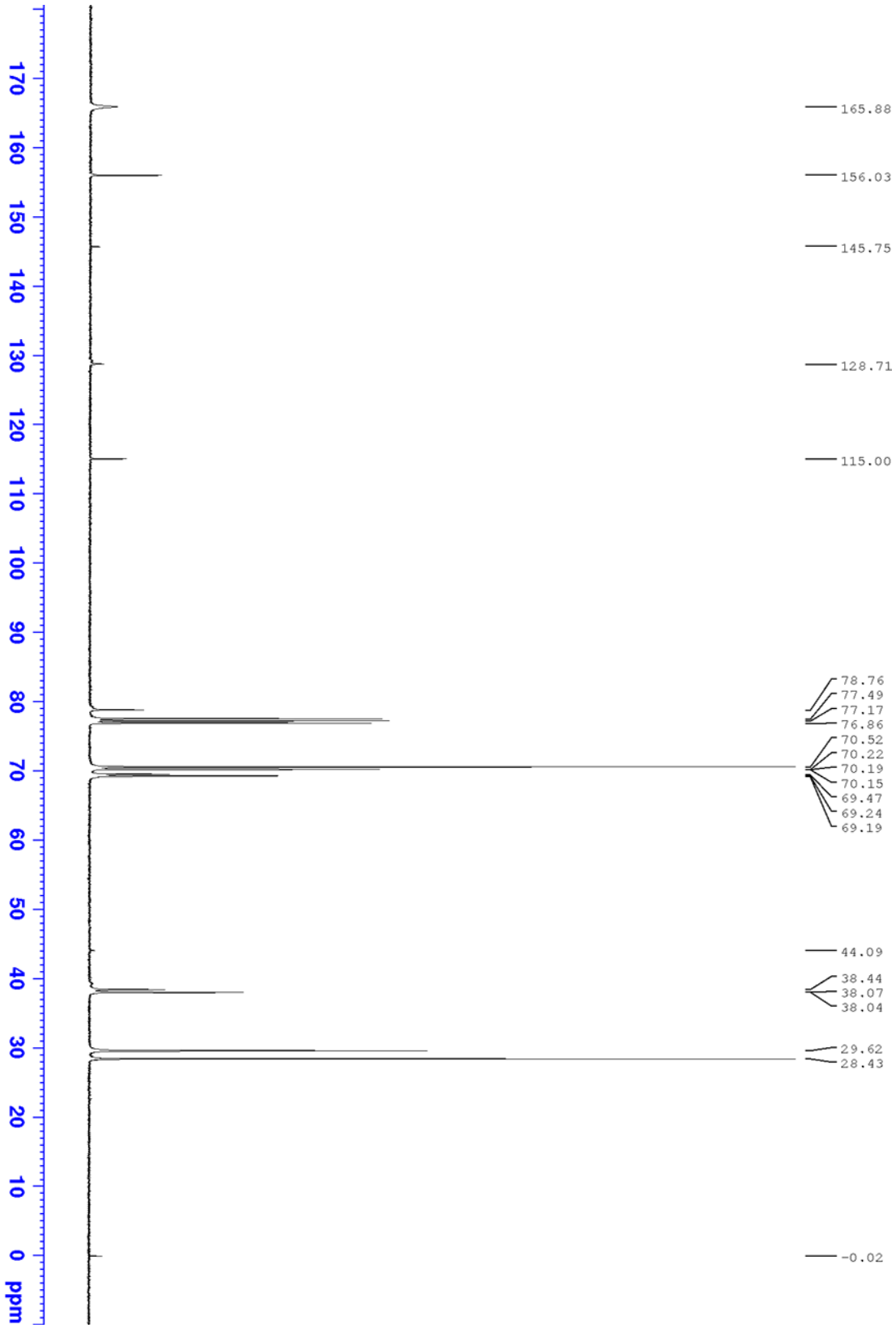

SI Figure 9 - Mass Spectra of G2 Aniline Dendron

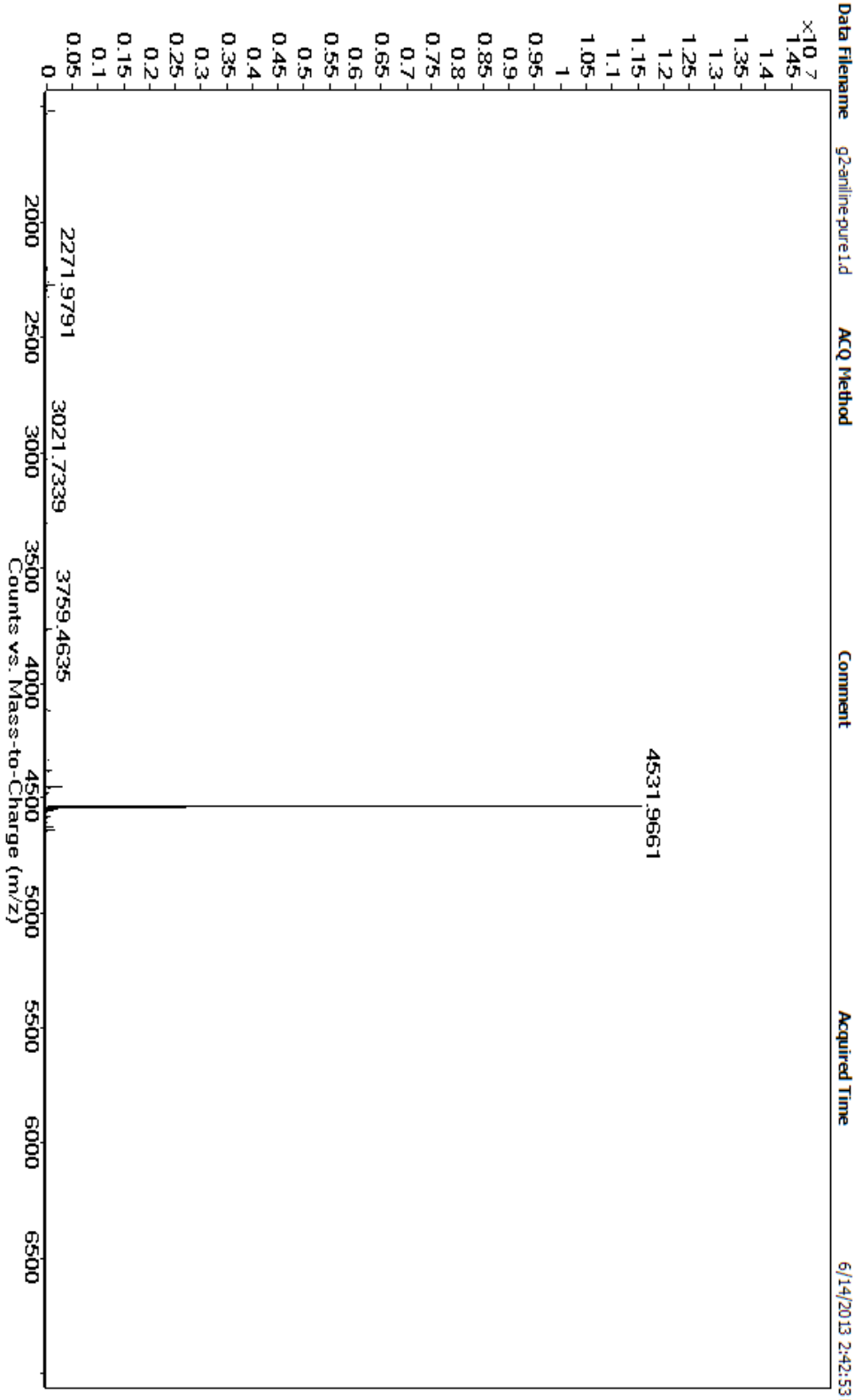

G0-Diazonium

$H[AuCl_4]•3H_2O$ (0.094 g, 0.240 mmol) and $[NO]PF_6$ (0.042 g, 0.240 mmol) were added to a solution of **G0-aniline** (0.200 g, 0.240 mmol) in CD_3CN (2.4 mL) while stirring. The reaction was kept at 0ºC for 4 hours and was left to reach room temperature in a 2 hours period time. The crude product was purified by precipitation acetonitrile/ diethyl ether and evaporated under vacuum to give **G0-diazonium** (0.227 g, 80%) as a dark brown solid. ^{1}H NMR (400 MHz, CD_3CN) δ 8.49-8.47 (dd, J = 8.4 Hz, 2H, m-diazobenzene), 7.89 (dd, J = 8.6 Hz, 2H, o-diazobenzene), 4.81 (br, 2H, aniline-C**H**$_2$-NH-triazine) 3.69-3.43 (m, 28H, C**H**$_2$OC**H**$_2$C**H**$_2$OC**H**$_2$C**H**$_2$OC**H**$_2$, C_3N_3-NHC**H**$_2$$CH_2CH_2O$), 3.18 (br m, 4H, BocNHC**H**$_2$), 2.0-1.7 (br m, 8H, OCH_2C**H**$_2$$CH_2$); ^{13}C NMR (100 MHz, CD_3CN) δ 155.2 (**C**$_3$N$_3$), 132.6 (o-aryldiazo), 130.3 (m-aryldiazo), 120.5 (N_2-**C**(ipso)), 69.2 (O**C**H_2**C**H_2O), 68.3 (two lines, CH_2CH_2**C**H_2O), 40.5 (aryldiazo-**C**H_2-NH-triazine), 38.6 (**C**$H_2CH_2CH_2O$), 38.4 (**C**$H_2CH_2CH_2O$) 28.3 ($NHCH_2$**C**H_2CH_2O), 27.8 ($NHCH_2$**C**H_2CH_2O).

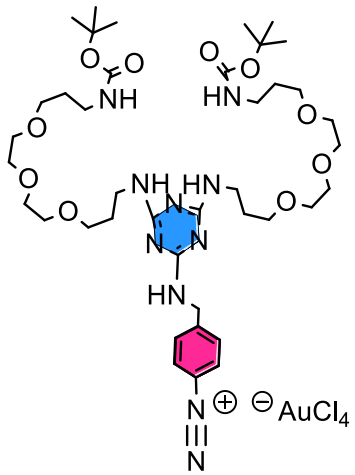

SI Figure 10 - ^{1}H NMR of G0-Diazonium Dendron (CD_3CN)

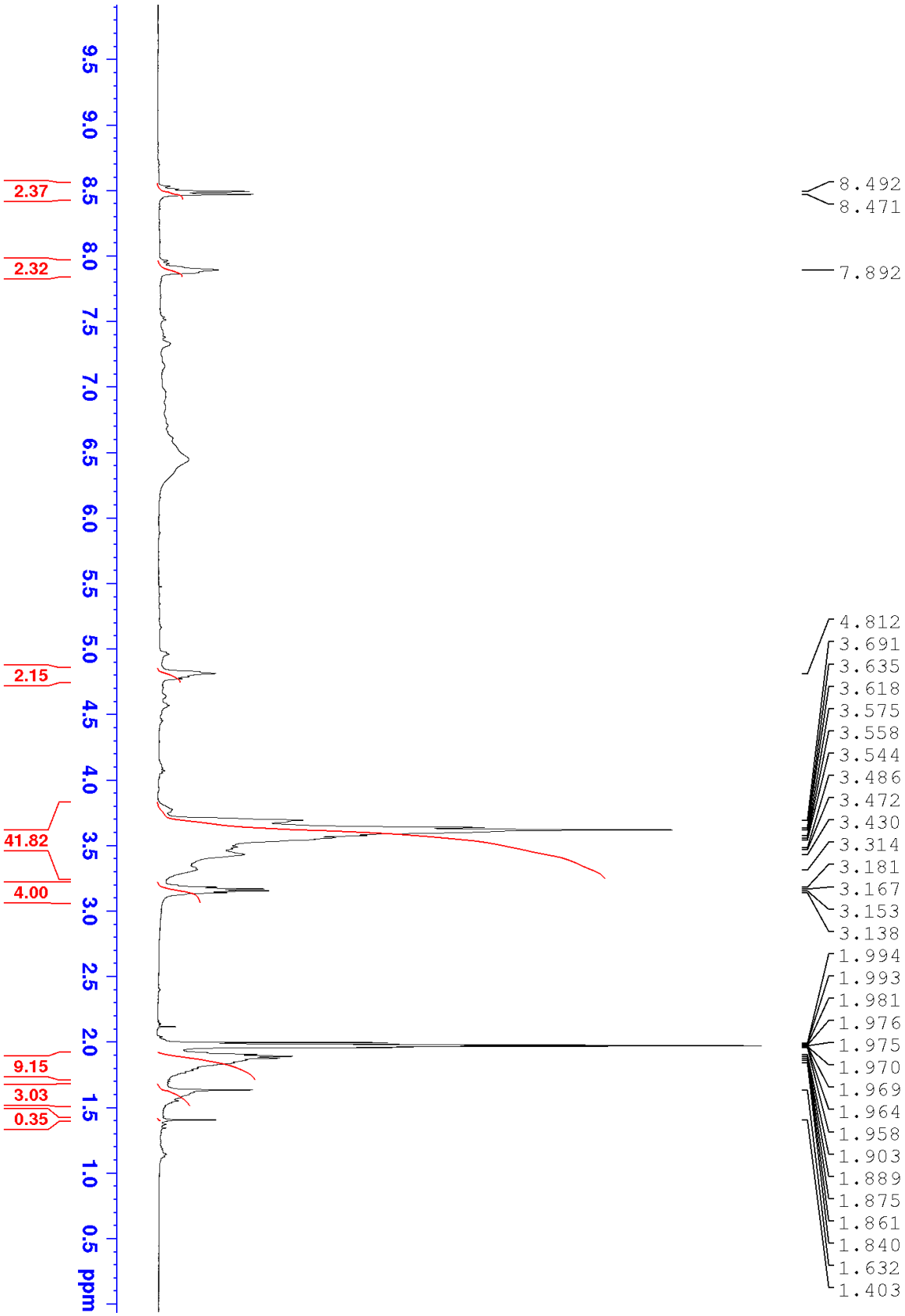

SI Figure 11 - ^{1}H NMR of G0-Diazonium Dendron (CD_3CN + CD_3OD)

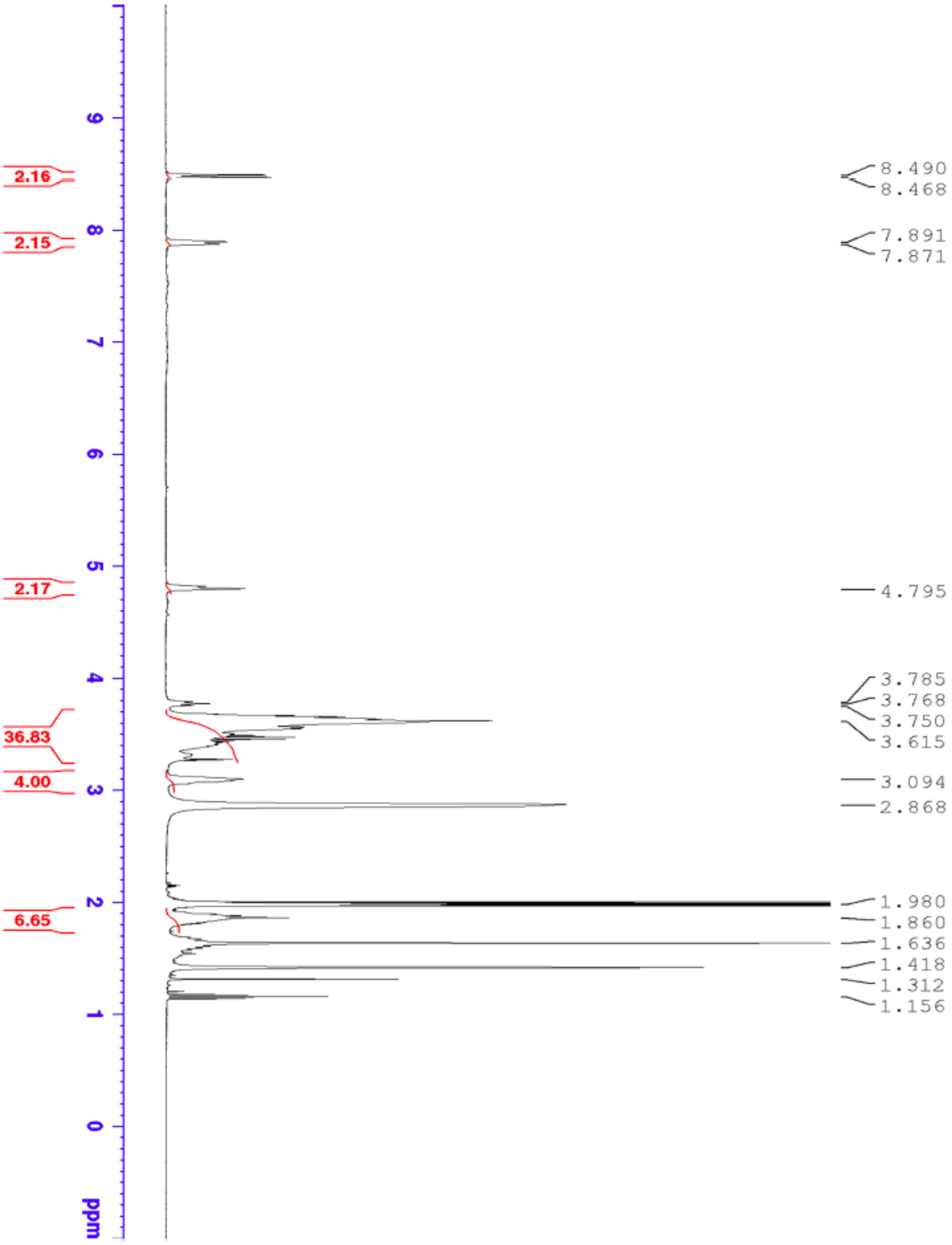

SI Figure 12 - ^{13}C NMR of G0- Diazonium Dendron

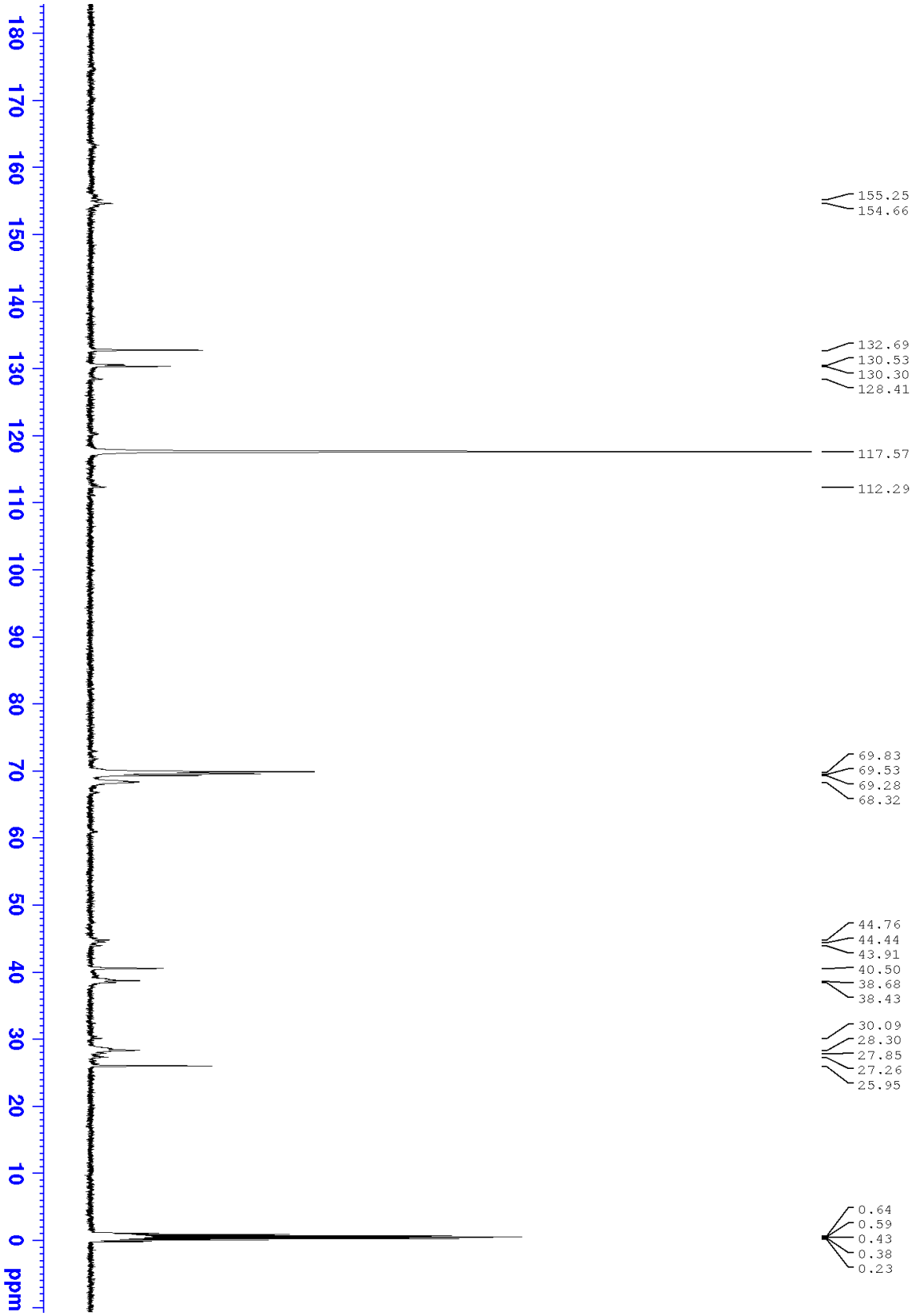

G1-diazonium

$H[AuCl_4]•3H_2O$ (0.057 g, 0.145 mmol) and $[NO]PF_6$ (0.045 g, 0.261 mmol) were added to a solution of **G1-aniline** (0.300 g, 0.145 mmol) in CD_3CN (2.5 mL) while stirring. The reaction was kept at 0ºC for 4 hours and was left to reach room temperature in a 2 hours period time. The crude product was purified by precipitation acetonitrile/ diethyl ether and evaporated under vacuum to give **G1-diazonium** (0.248 g, 71%) as a reddish-brown solid. ^{1}H NMR (400 MHz, CD_3CN) δ 8.5-8.48 (dd, J = 8.4 Hz, 2H, m-diazobenzene), 7.89 (dd, J = 8.6 Hz, 2H, o-diazobenzene), 4.79 (br, 2H, aniline-C**H**$_2$-NH-triazine) 3.59-3.57 (m, 88H, C**H**$_2$OC**H**$_2$C**H**$_2$OC**H**$_2$C**H**$_2$OC**H**$_2$, C_3N_3-NHC**H**$_2$$CH_2CH_2O$), 3.09 (br m, 8H, BocNHC**H**$_2$), 1.9-1.8 (br s, 24H, OCH_2C**H**$_2$$CH_2$)), 1.63/1.41 (s, 36H, C(C**H**$_3$)$_3$);^{13}C NMR (100 MHz, CD_3CN) δ 154.9 (**C**$_3$N$_3$), 151.9 (**C**O), 132.7 (o-diazo), 130.3 (m-diazo),122.8 (N$_2$-**C**(ipso)), 85.1 (**C**$(CH_3)_3$), 69.9 (OCH_2CH_2O), 69.8 (OCH_2CH_2O), 69.5 (OCH_2CH_2O), 68.6 ($CH_2CH_2CH_2O$), 68.2 ($CH_2CH_2CH_2O$), 40.5 (aryldiazo-**C**H_2-NH-triazine), 38.8 (**C**$H_2CH_2CH_2O$), 38.3 (**C**$H_2CH_2CH_2O$), 28.9 ($NHCH_2CH_2CH_2O$), 28.3 ($NHCH_2CH_2CH_2O$), 27.7 (**C**$(CH_3)_3$). *Note: The peaks at 1.41 and 1.63 are tentatively assigned as 50% of the BOC signal each. This behavior has been seen in other species, but not those so remote from the core.*

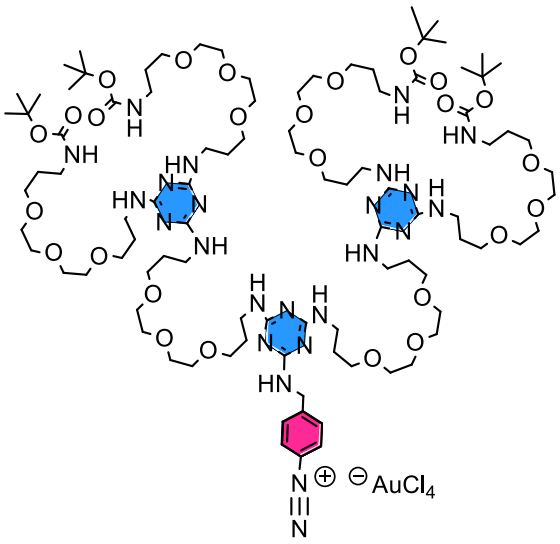

SI Figure 13 - ^{1}H NMR of G1-Diazonium Dendron (CD_3CN)

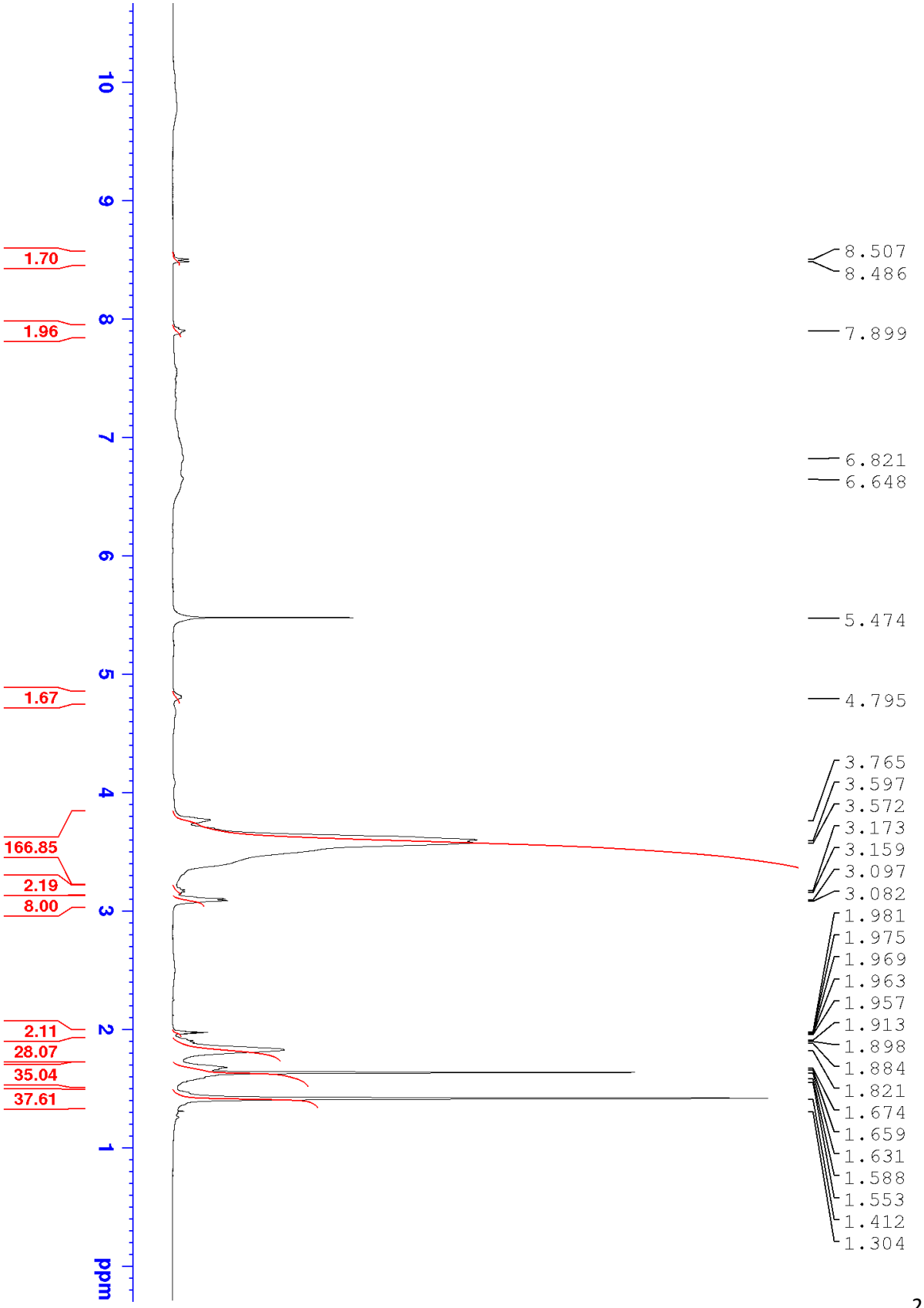

SI Figure 14 - ^{1}H NMR of G1-Diazonium Dendron (CD_3CN+CD_3OD)

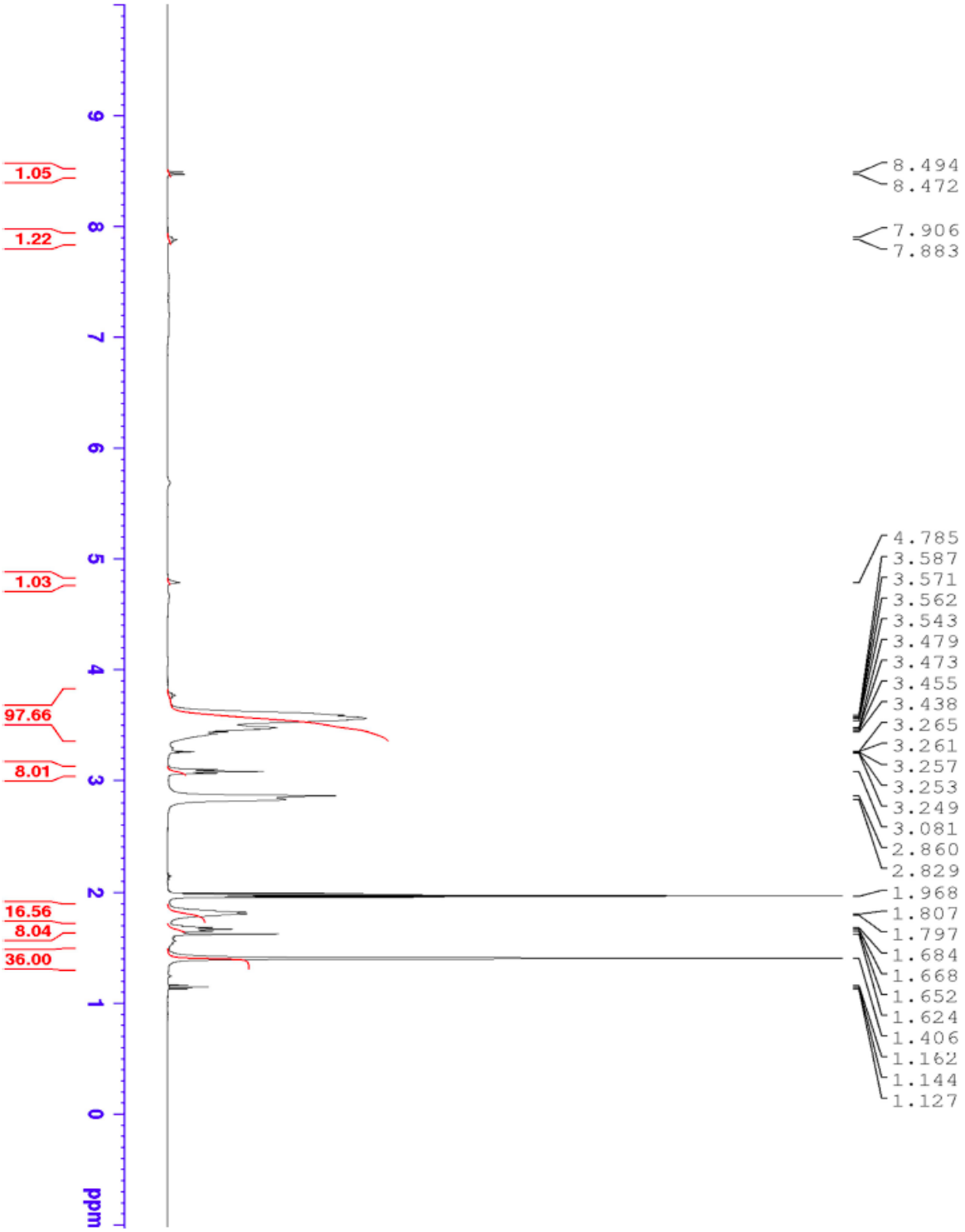

SI Figure 15 - ^{13}C NMR of G1 Diazonium Dendron

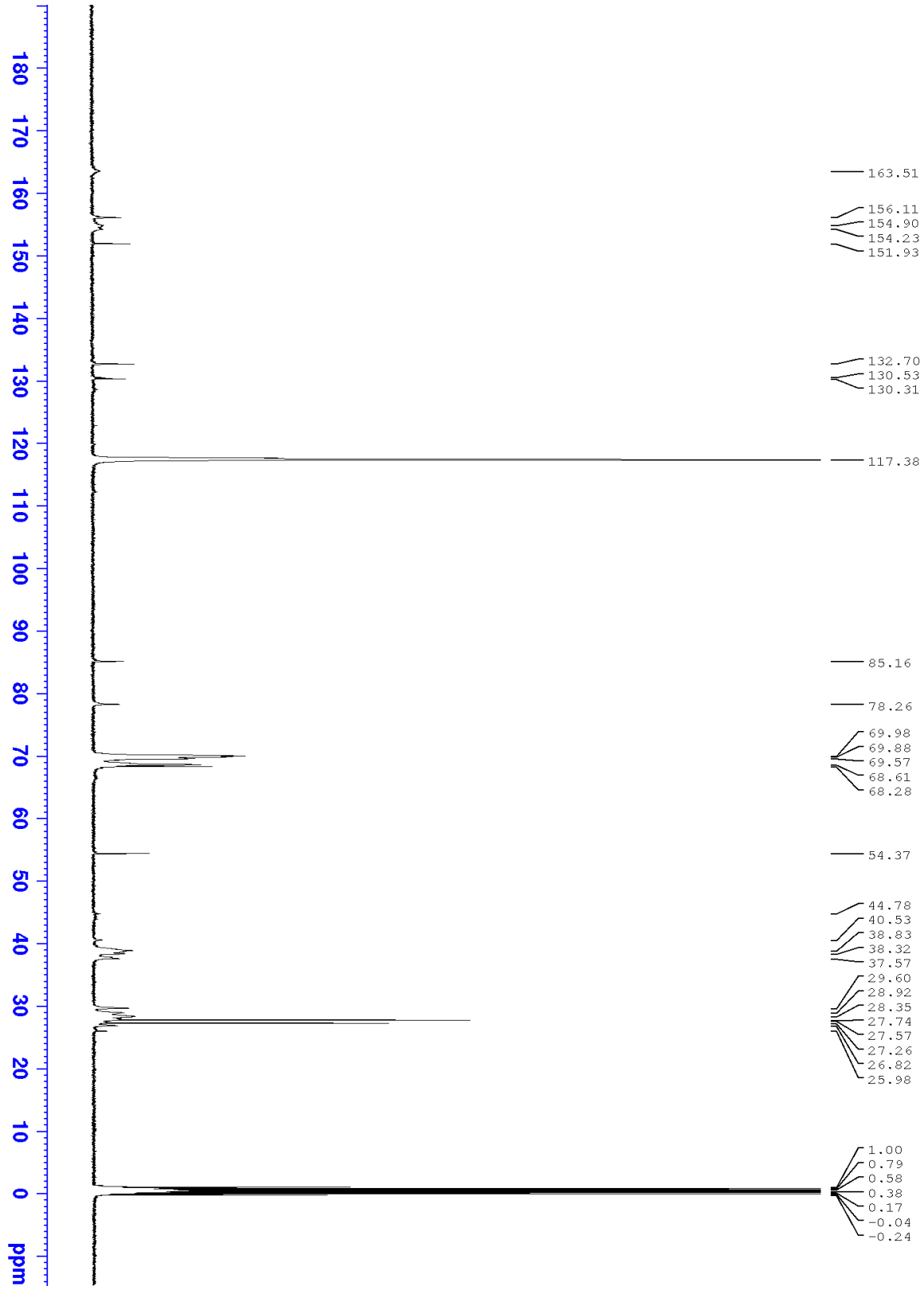

G2-diazonium

$H[AuCl_4]•3H_2O$ (0.130 g, 0.029 mmol) and $[NO]PF_6$ (0.010 g, 0.058 mmol) were added to a solution of **G2-aniline** (0.130 g, 0.029 mmol) in CD_3CN (1 mL) and dioxane (0.2 mL) while stirring. The reaction was kept at 0ºC for 4 hours and was left to reach room temperature in a 2 hours period time. The crude product was purified by precipitation acetonitrile/ diethyl ether and evaporated under vacuum to give **G2-diazonium** (0.088 g, 62%) as a reddish-brown solid. ^{1}H NMR (400 MHz, CD_3CN) δ 8.48 (dd, J = 8.4 Hz, 2H, m-diazobenzene), 7.89 (dd, J = 8.6 Hz, 2H, o-diazobenzene), 4.80 (br, 2H, aniline-C**H**$_2$-NH-triazine) 3.80-3.41 (m, 208H, C**H**$_2$OC**H**$_2$C**H**$_2$OC**H**$_2$C**H**$_2$OC**H**$_2$, C_3N_3-NHC**H**$_2$$CH_2CH_2O$), 3.10 (br m, 16H, BocNHC**H**$_2$), 1.9-1.7 (m, 56H, OCH_2C**H**$_2$$CH_2$)), 1.63/1.41 (s, 72H, C(C**H**$_3$)$_3$);^{13}C NMR (100 MHz, CD_3CN) δ 154.3 (**C**$_3$N$_3$), 151.9 (**C**O), 132.7 (o-diazo), 130.3 (m-diazo),122.8 (N_2-**C**(ipso)), 85.1 (**C**$(CH_3)_3$), 70.0 (O**C**H_2**C**H_2O), 69.8 (O**C**H_2**C**H_2O), 69.7 (O**C**H_2**C**H_2O), 69.5 (O**C**H_2**C**H_2O), 68.6 (CH_2CH_2**C**H_2O), 68.3 (CH_2CH_2**C**H_2O), 40.5 (aryldiazo-**C**H_2-NH-triazine), 38.7 (**C**$H_2CH_2CH_2$O), 38.3 (**C**$H_2CH_2CH_2$O), 28.9 (NHCH_2**C**H_2CH_2O), 28.4 (NHCH_2**C**H_2CH_2O), 27.2 (C(**C**H_3)$_3$). *Note: The peaks at 1.41 and 1.63 are tentatively assigned as 50% of the BOC signal each. This behavior has been seen in other species, but not those so remote from the core.*

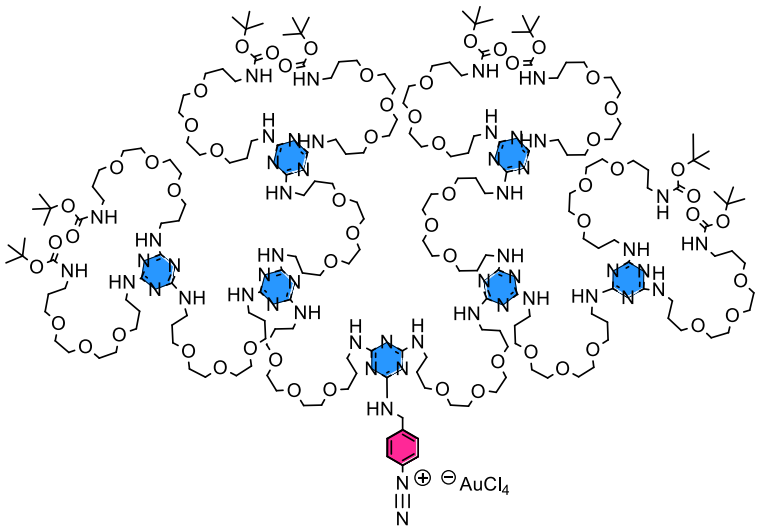

SI Figure 16 - ^{1}H NMR of G2-Diazonium Dendron (CD_3CN)

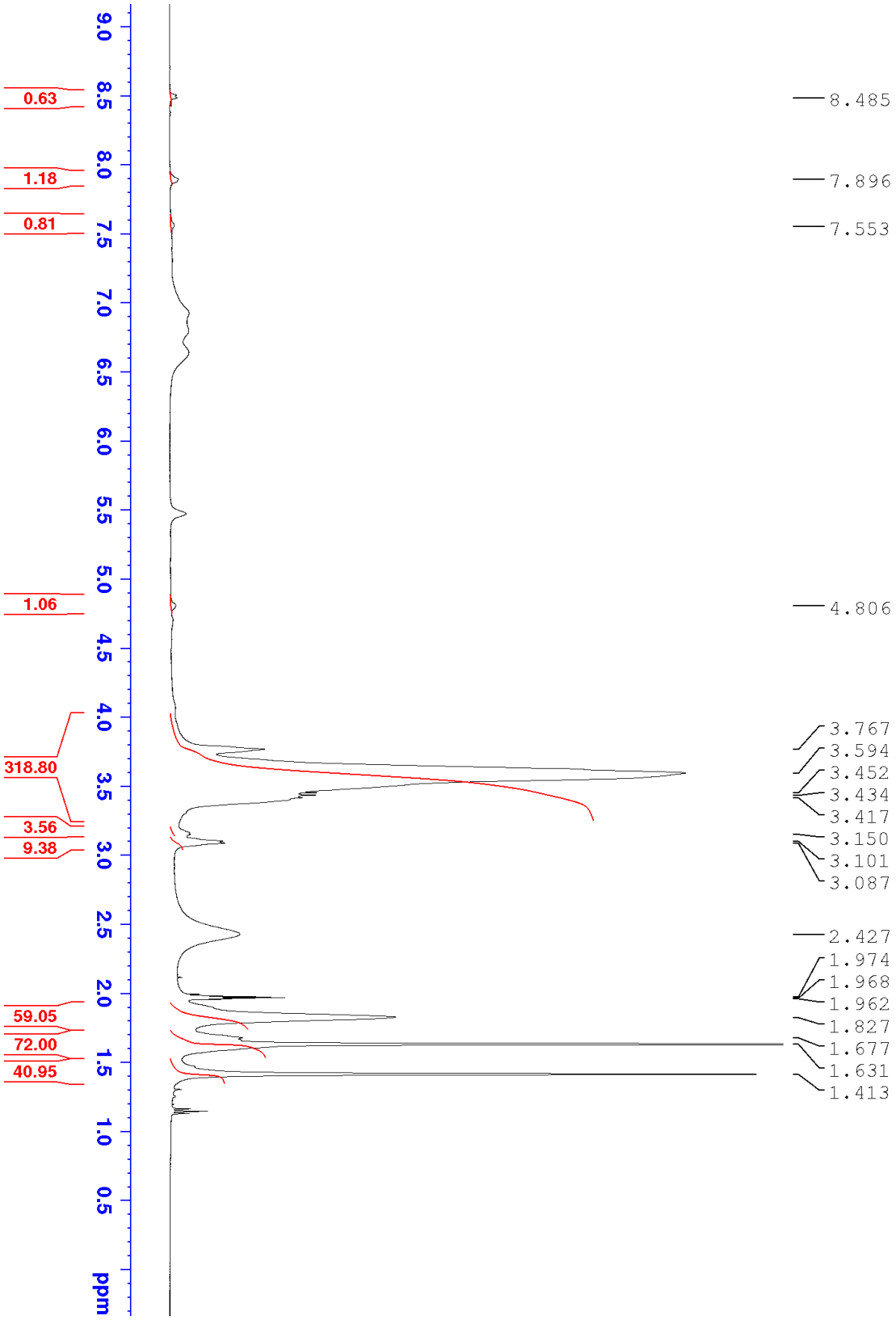

SI Figure 17 - ^{1}H NMR of G2-Diazonium Dendron (CD_3CN + CD_3OD)

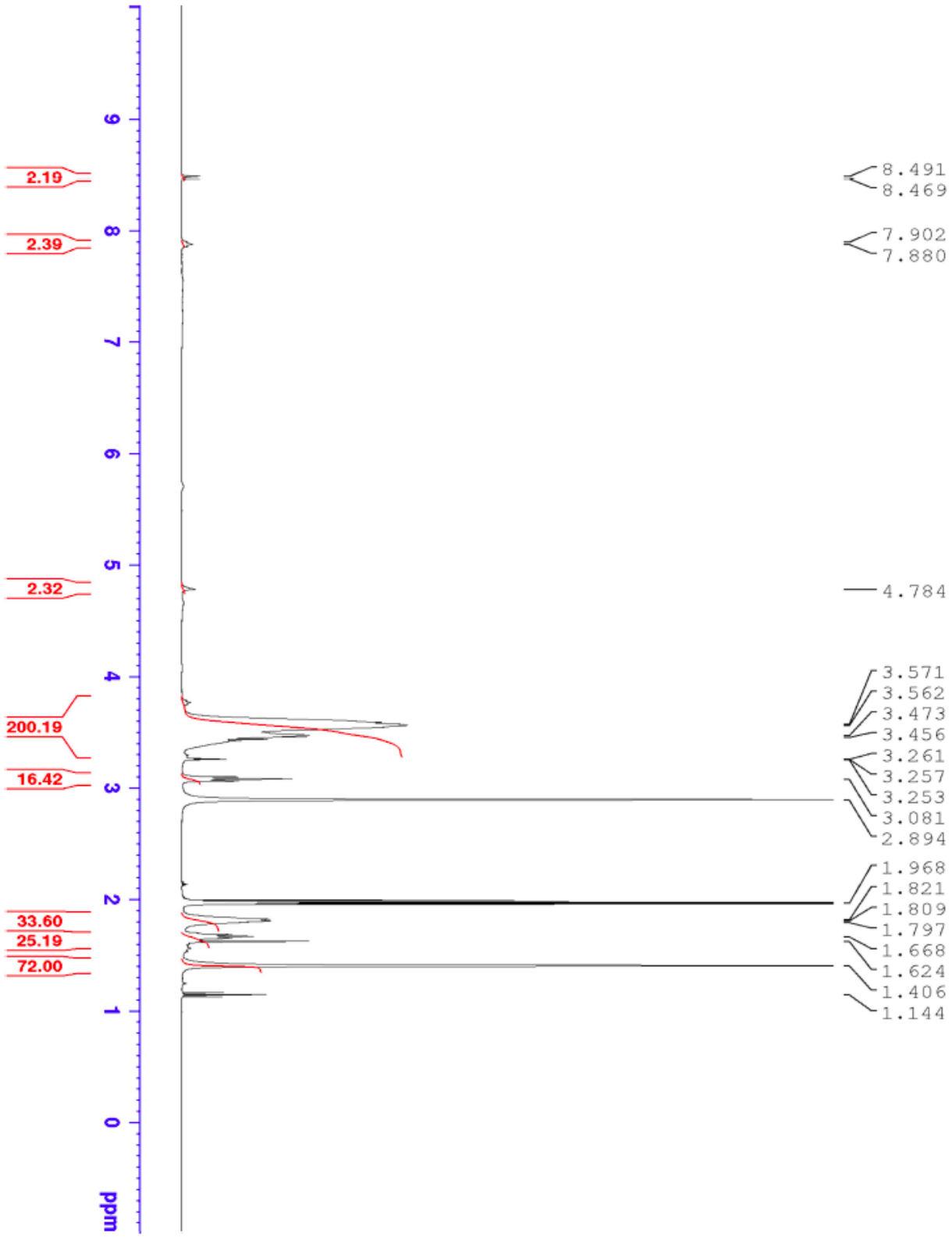

SI Figure 18 - ^{13}C NMR of G2- Diazonium Dendron

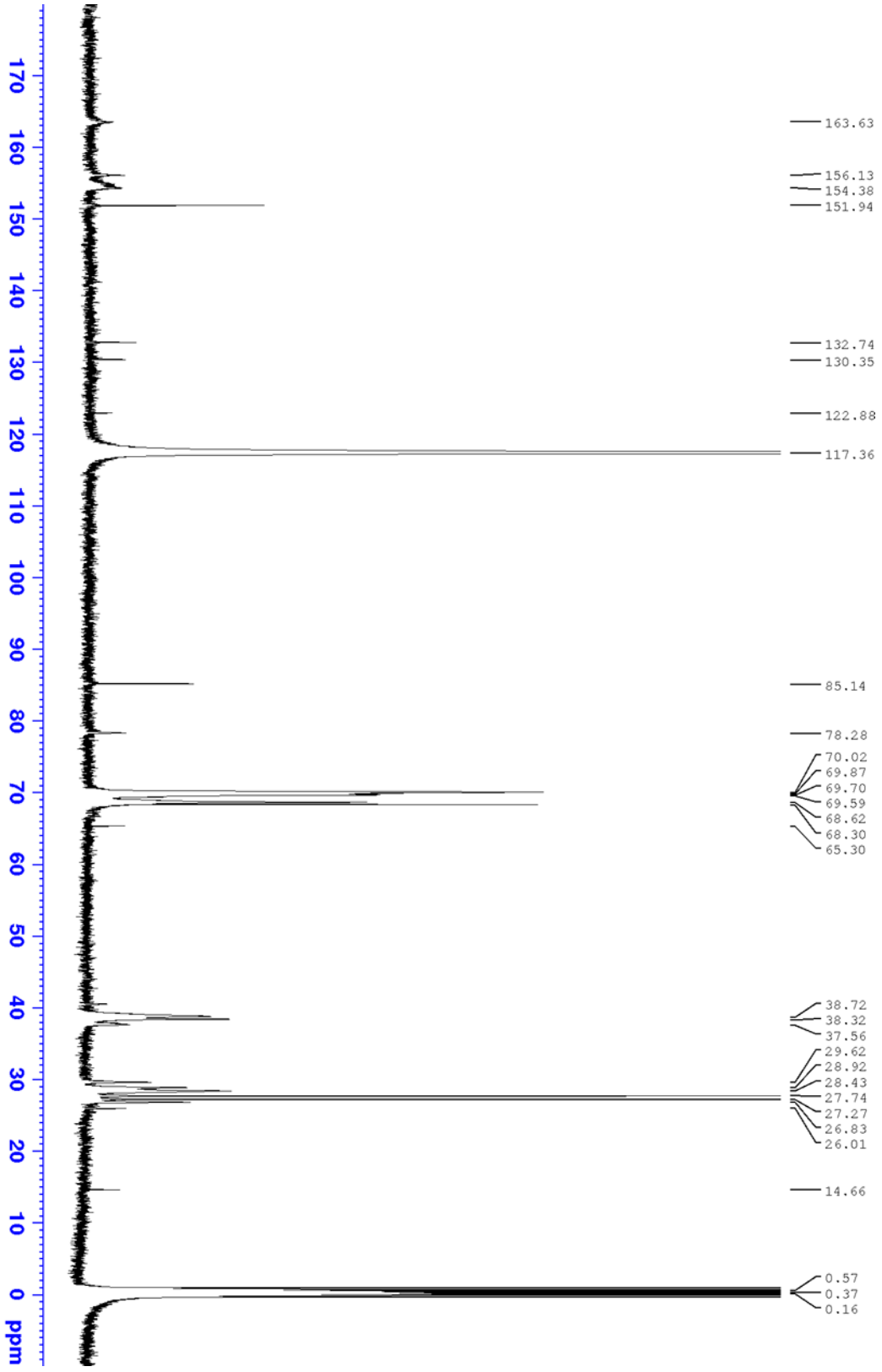

G0@AuNP

A solution 0.1 M of sodium borohydride (1mL) in acetonitrile was added over 1 hour to a solution of **G0-diazonium** (0.107 g, 0.084mmol) in 4mL of acetonitrile with vigorous stirring. During this time the solution turned deep purple. After the addition was complete, an equal volume of diethyl ether was added and the solution was passed through a Büchner funnel with a sintered glass disc "F." The yellow filtrate was discarded. After washing the collected gummy solid several times with acetonitrile:diethyl ether, the solid was mixed with acetonitrile and centrifuged for 20 minutes at 3400RPM. The solution was removed from the pellet with a glass pipet, and the pellet was discarded. This solution could be stored or the solvent could be evaporated to provide a solid.

BOC- G0@AuNP

G0@AuNP (48mg) was mixed with BOC-anhydride (50mg, 229μM), and DIPEA (0.02mL, 114μM) in 0.6 mL of MeOH. The reaction was stirred overnight. After removing the methanol with a rotary evaporator, the residue was dissolved in dichloromethane and the organic phase was washed with three portions of water. The organic phase was removed and the residue was stirred with a 1:1 mixture of ether:acetonitrile, passed through a Büchner funnel with a sintered glass disc "F," and then remaining solid was collected for use.

SI Figure 19 - ^{1}H NMR in Acetonitrile of G0@AuNP- deprotected

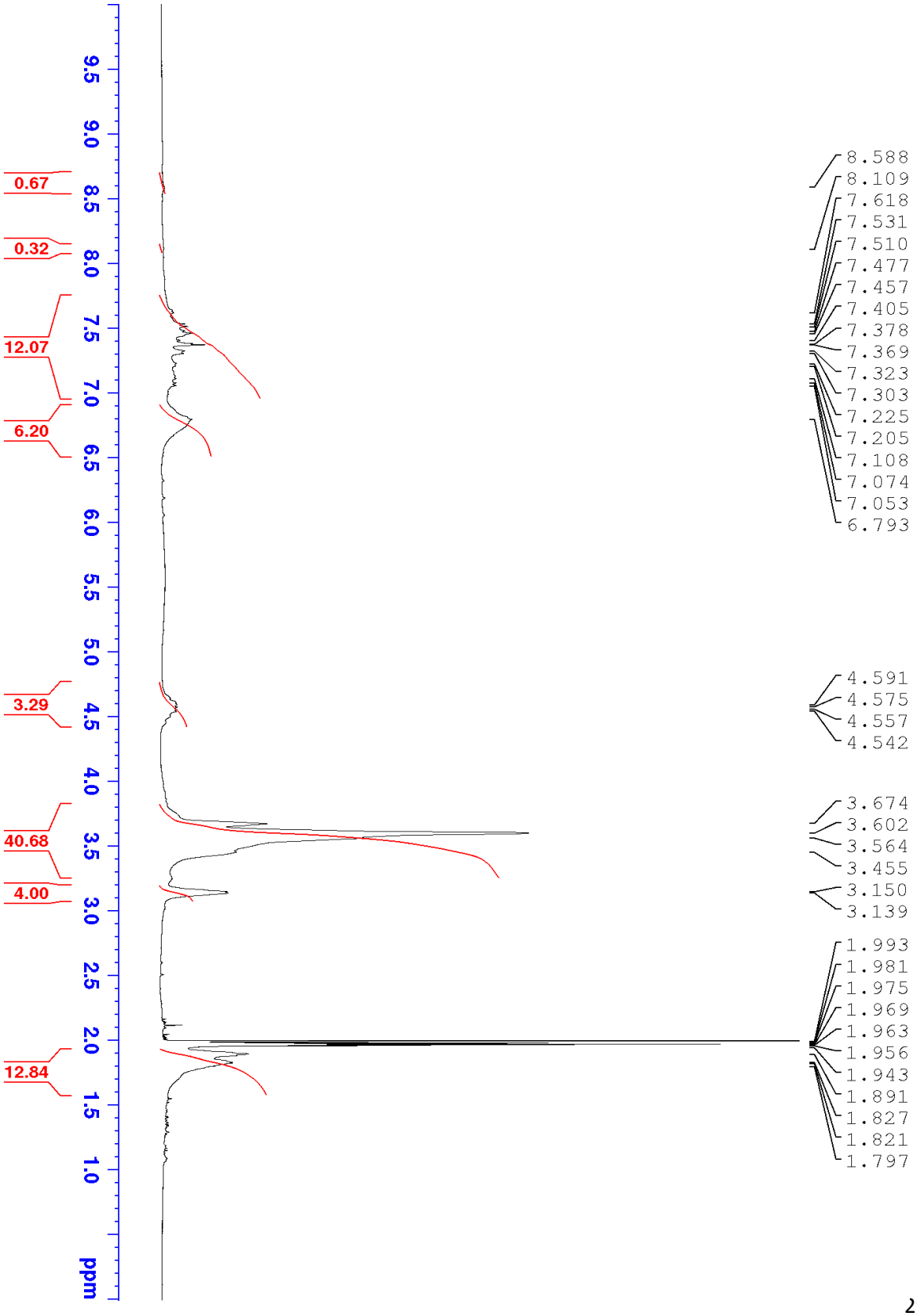

SI Figure 20 - ^{13}C NMR in Acetonitrile of G0@AuNP- deprotected

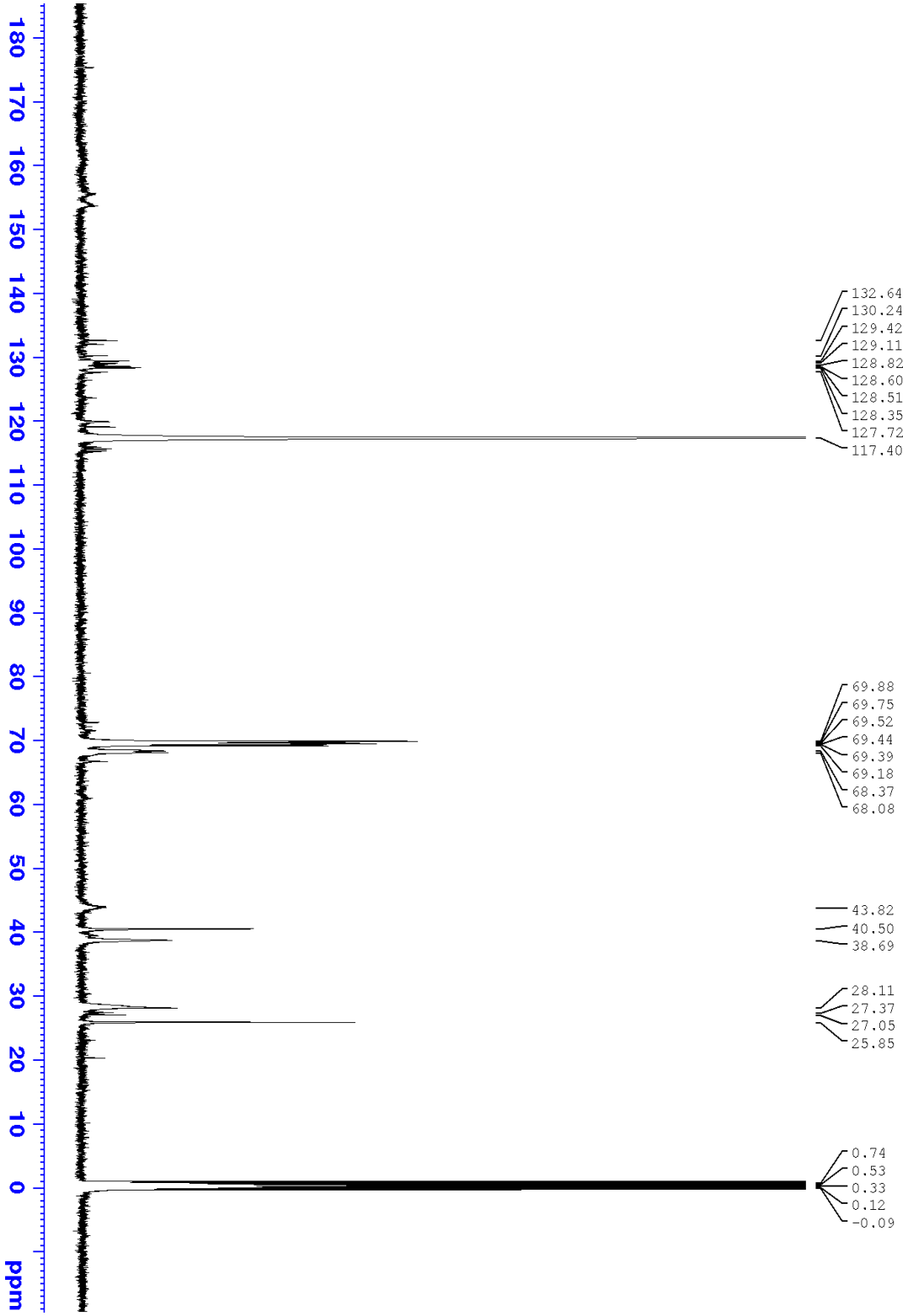

SI Figure 21 - ^{1}H NMR in $CDCl_3$ of BOC-G0@AuNP

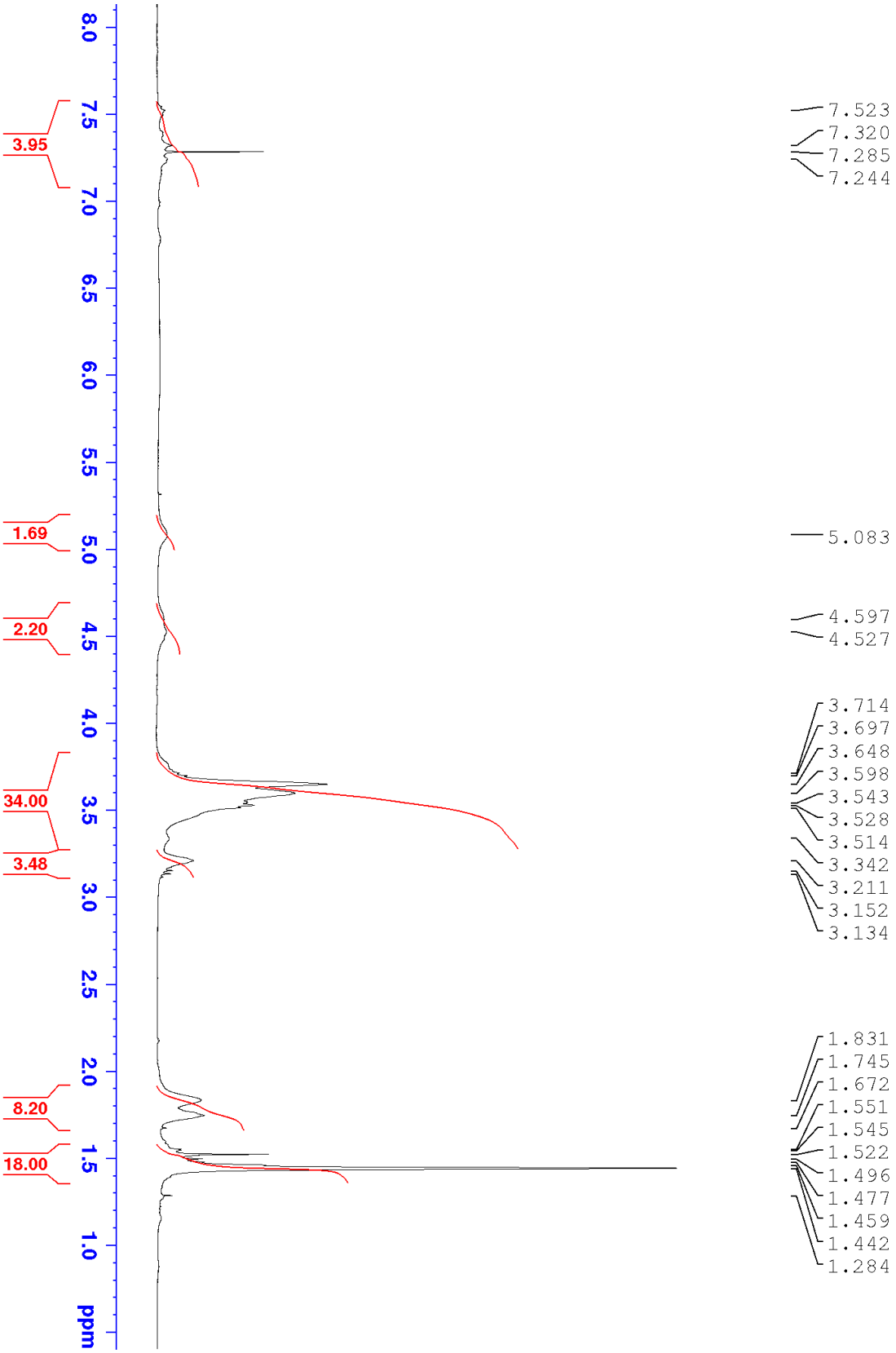

SI Figure 22 - ^{13}C NMR in $CDCl_3$ of BOC-G0@AuNP

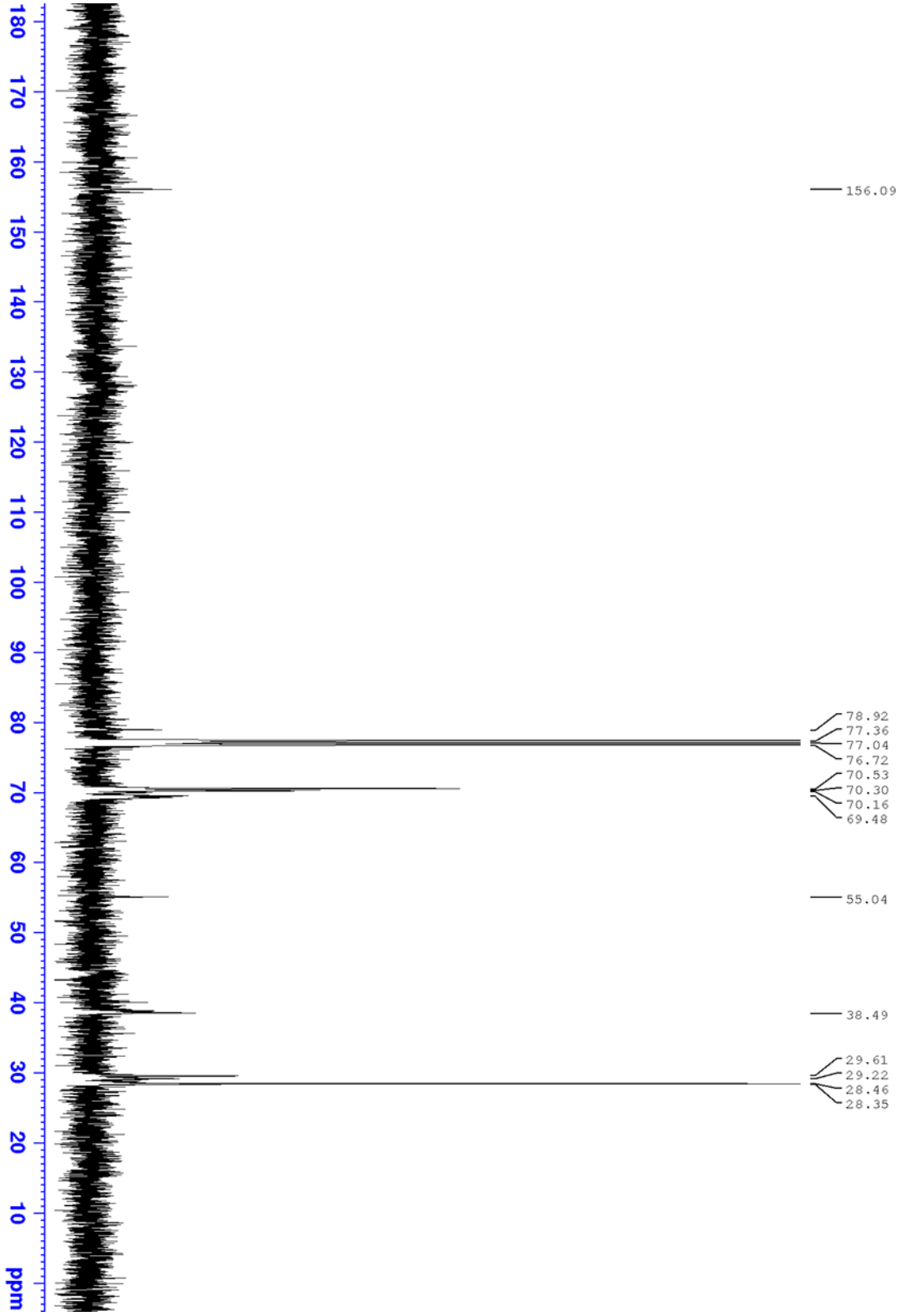

G1@AuNP

A solution 0.1 M of sodium borohydride (1mL) in acetonitrile was added over 1 hour to a solution of **G1-diazonium** (0.100 g, 0.049mmol) in 3mL of acetonitrile with vigorous stirring. During this time the solution turned red ruby. After the addition was complete, the solution was centrifuged twice for 10 min at 1500 rpm. The acetonitrile was removed by evaporation and the residue was dissolved in dichloromethane and washed with water. The organic phase was dried and the solvent was removed. Deprotection was accomplished by stirring the residue overnight in a solution of DCM:TFA (1:1). Afterwards, portions of toluene were added and evaporated three times. The residue was used as obtained after the final evaporation.

SI Figure 23 - ^{1}H NMR of BOC-G1@AuNP

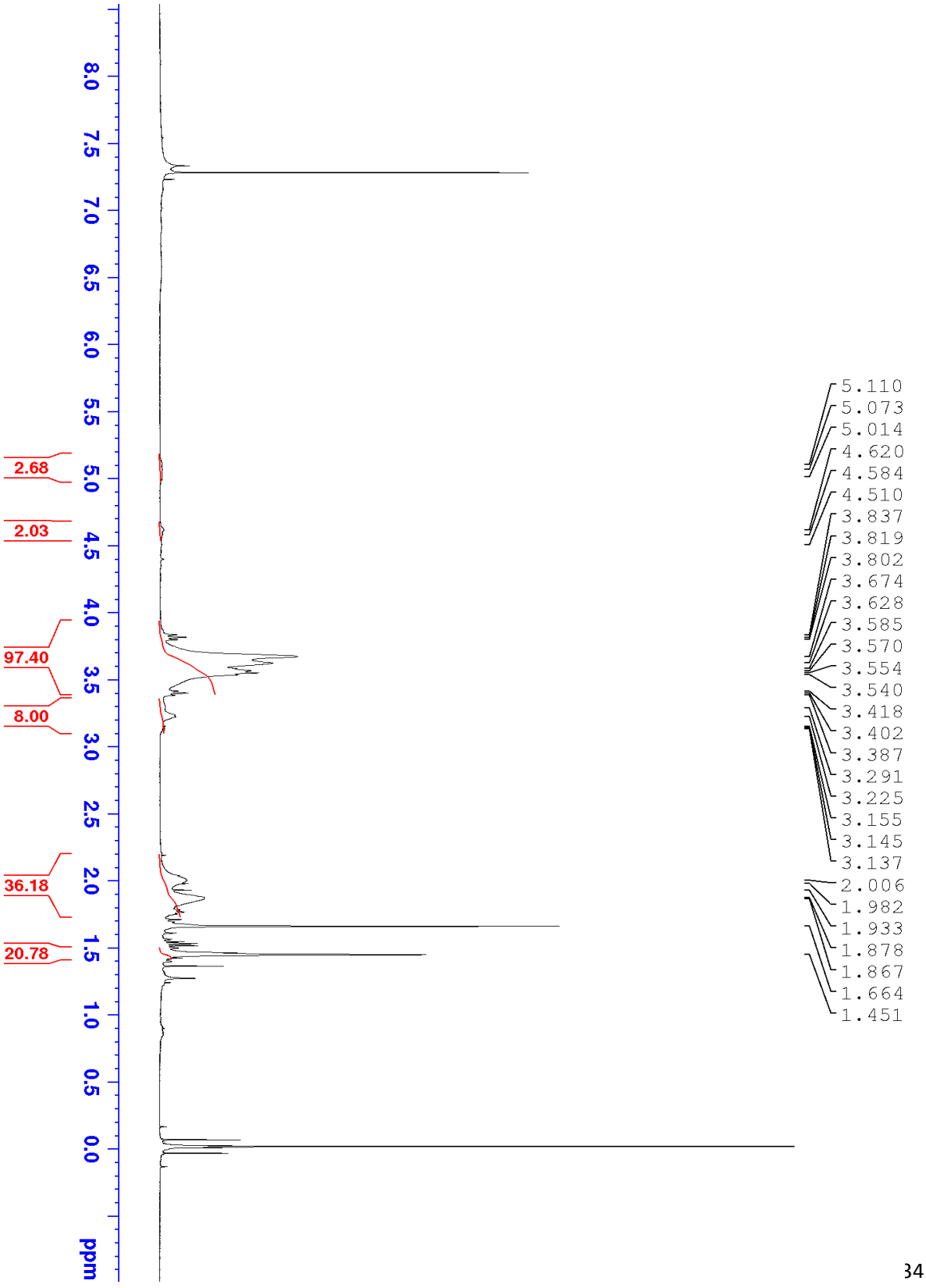

SI Figure 24 - ^{13}C NMR of BOC-G1@AuNP

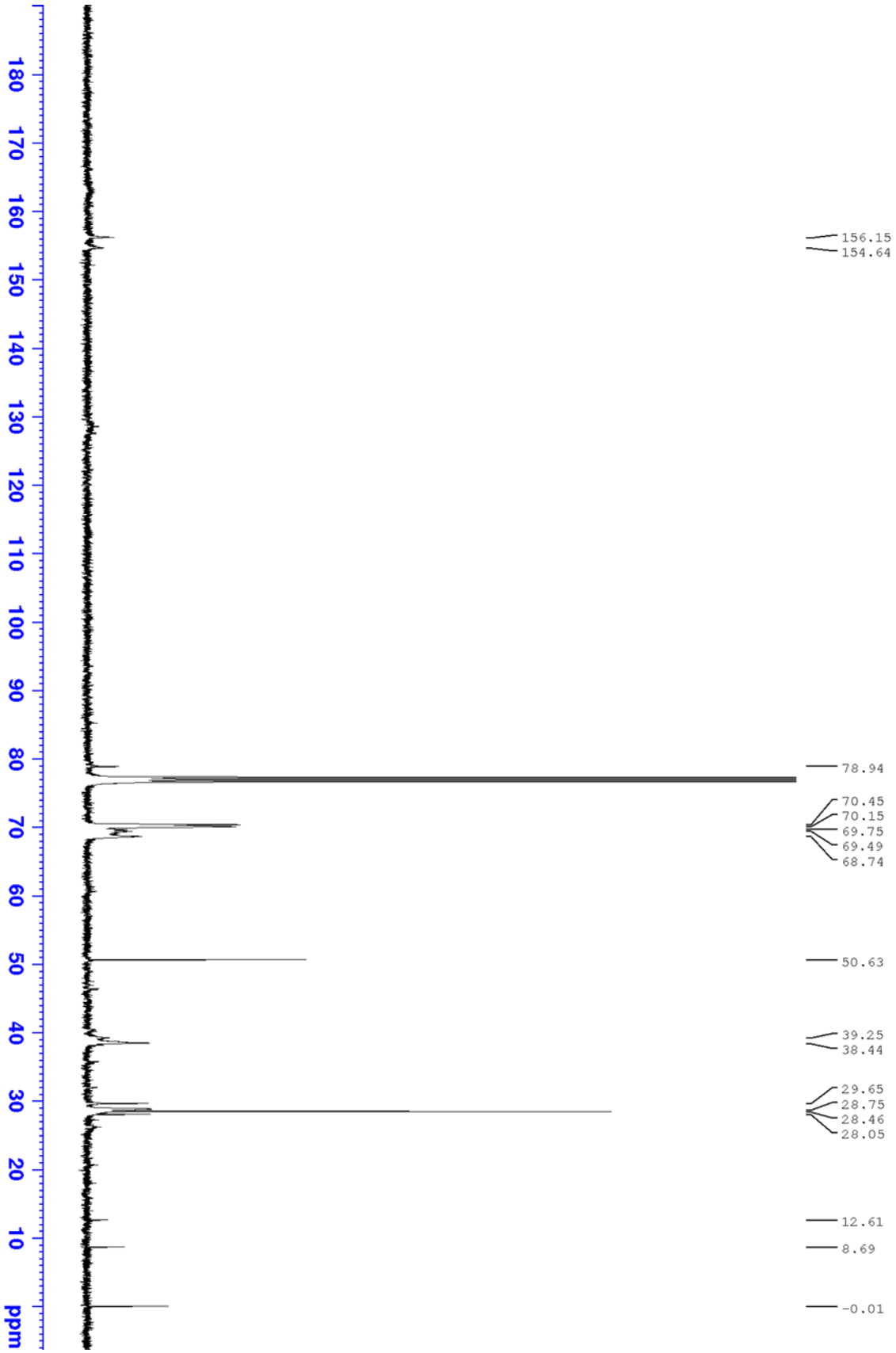

SI Figure 25 - ^{1}H NMR in D_2O of G1@AuNP- deprotected

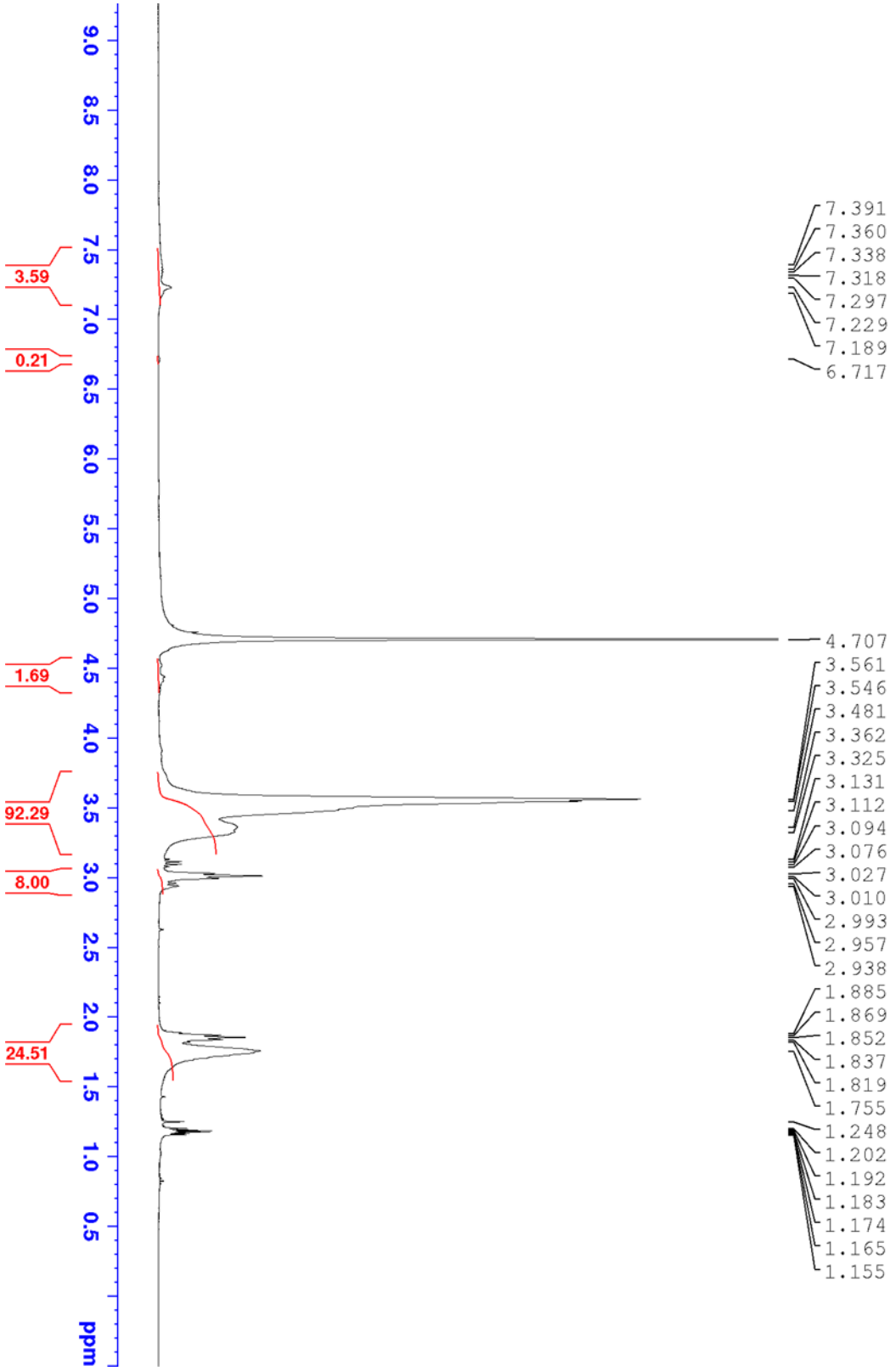

SI Figure 26 - ^{13}C NMR in D_2O of G1@AuNP- deprotected

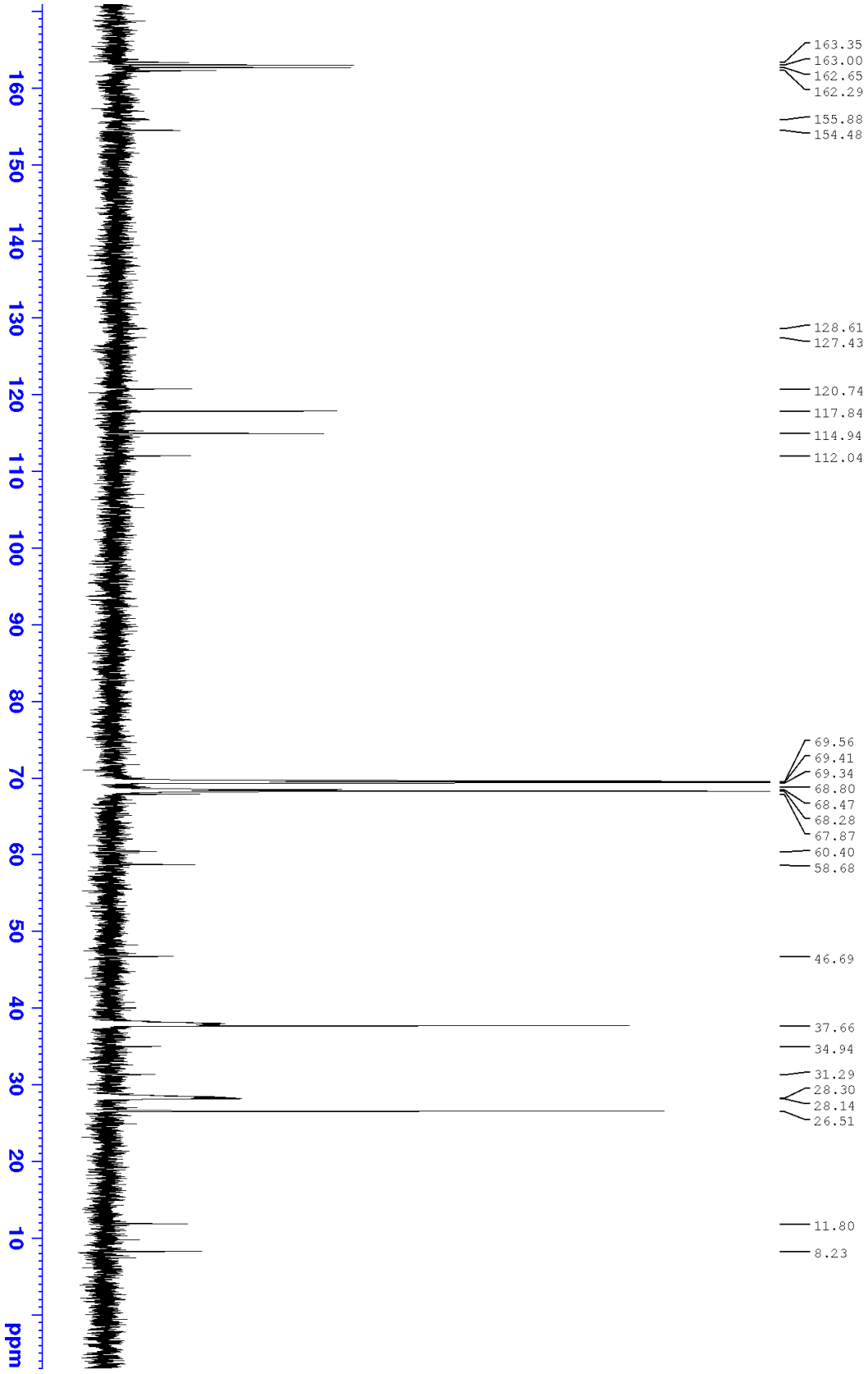

G2@AuNP

A solution 0.1 M of sodium borohydride (0.8 mL) in acetonitrile was added over 1 hour to a solution of **G2-diazonium** (0.088 g, 0.018mmol) in 2mL of acetonitrile with vigorous stirring. During this time the solution turned red ruby. After the addition was complete, an equal portion of diethyl ether was added and the solution was passed through a Büchner funnel with a sintered glass disc "F." After washing the collected solid several times with acetonitrile:diethylether. This solid was soluble in methanol. Deprotection was affected by stirring these particles overmight in a solution of DCM:TFA (1:1). Afterwards, portions of toluene were added and evaporated three times to yield the desired product.

SI Figure 27 - ^{1}H NMR in $CDCl_3$ of BOC-G2@AuNP

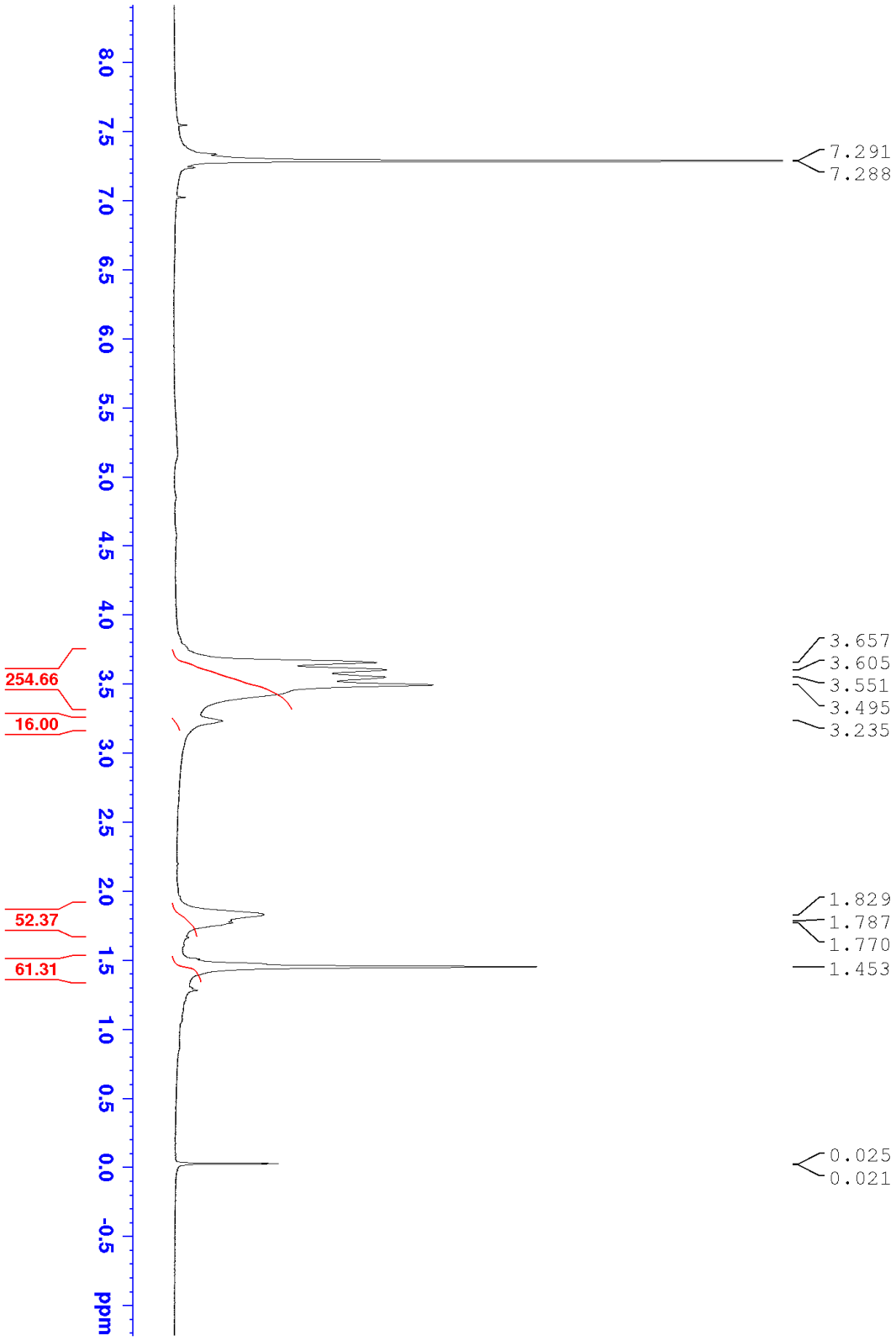

SI Figure 28 - ^{13}C NMR in MeOD of BOC-G2@AuNP

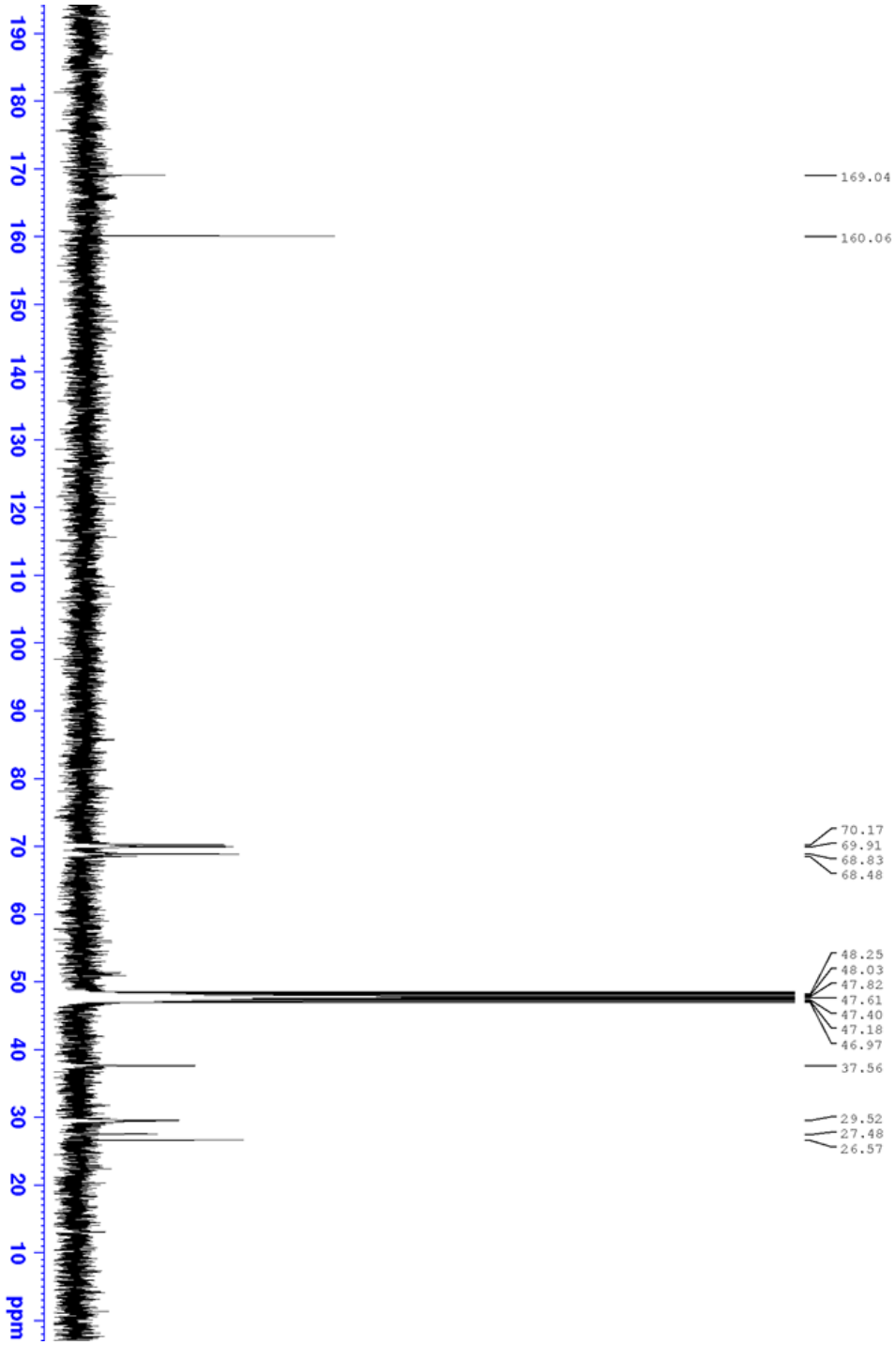

SI Figure 29 - ^{1}H NMR in D_2O of G2@AuNP- deprotected

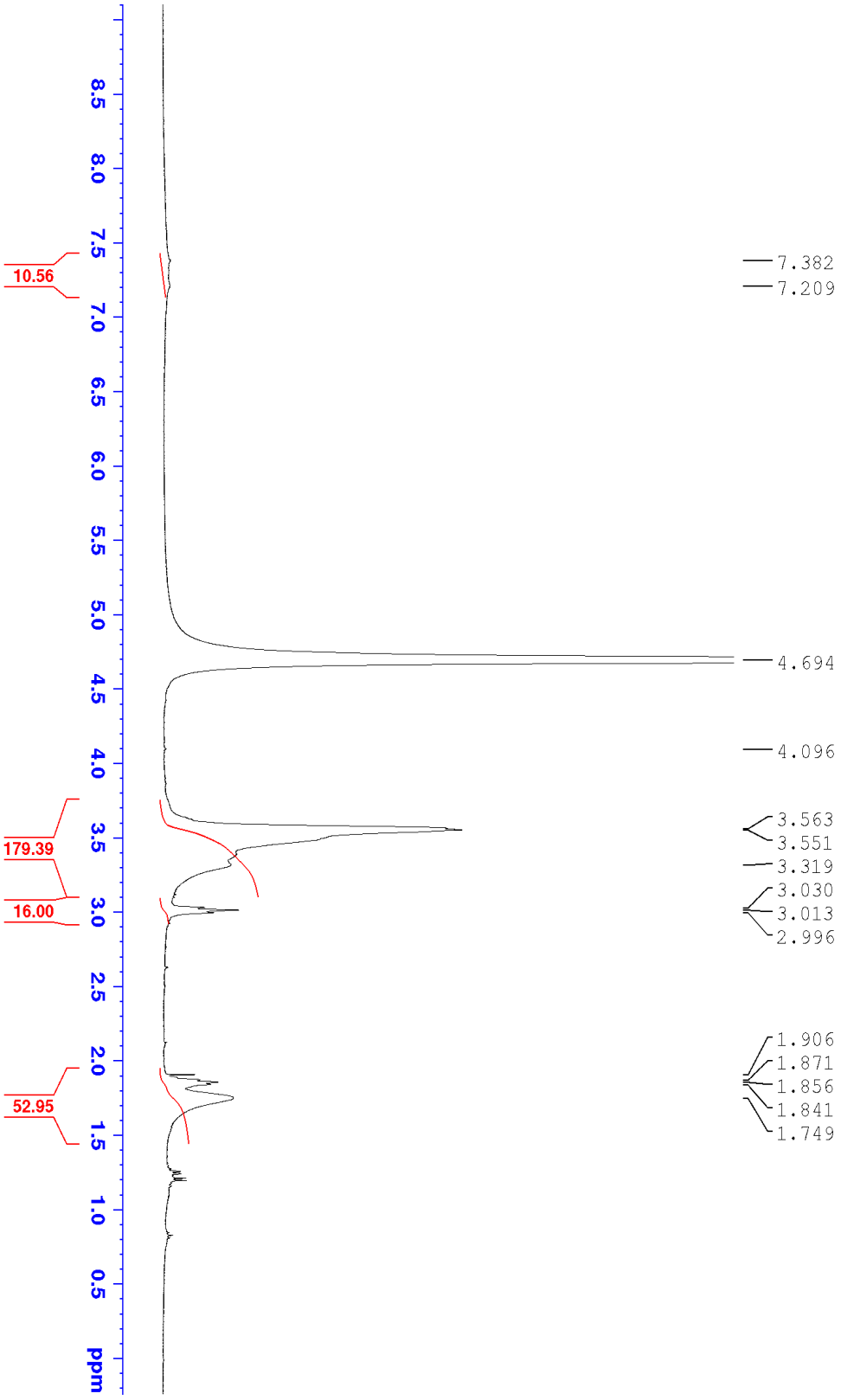

Figure 30 - ^{13}C

SI NMR in D_2O of G2@AuNP- deprotected

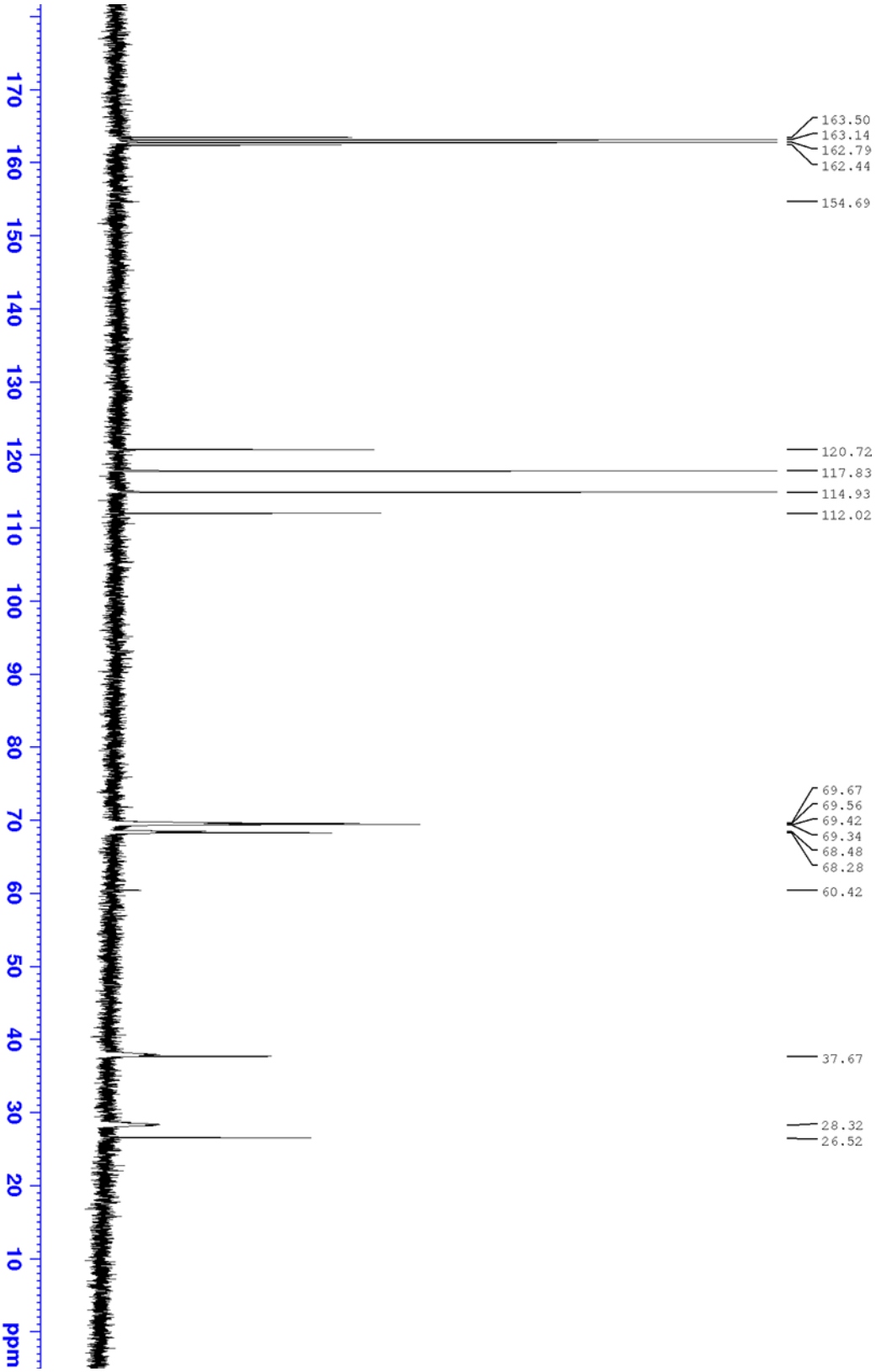

SI Figure 31 - IR of Dendrons containing diazonium moiety

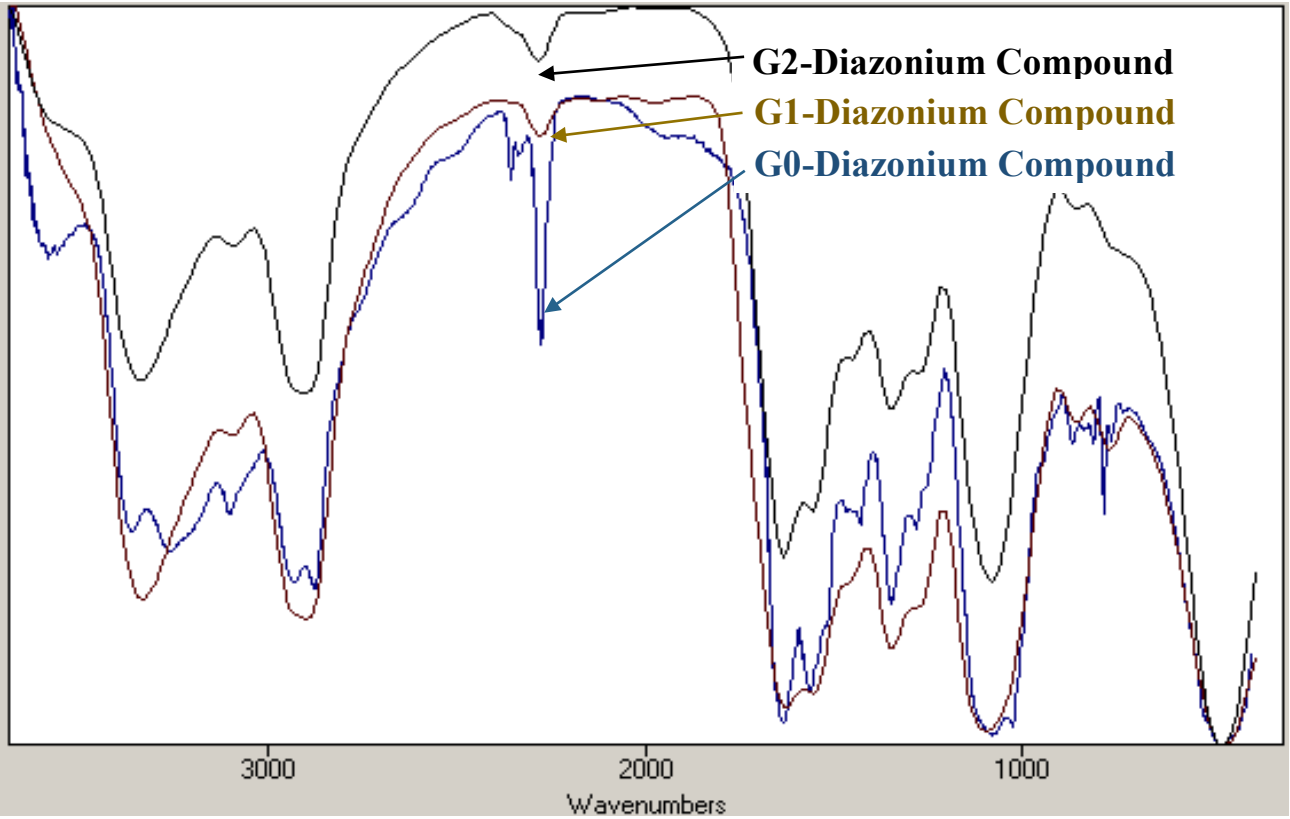

SI Figure 32. UV-vis spectra illustrating the reduction of the diazonium salt with a solution 0.1 M of $NaBH_4$ with formation of the plasmon band at 533 nm for G0@Au NPs.

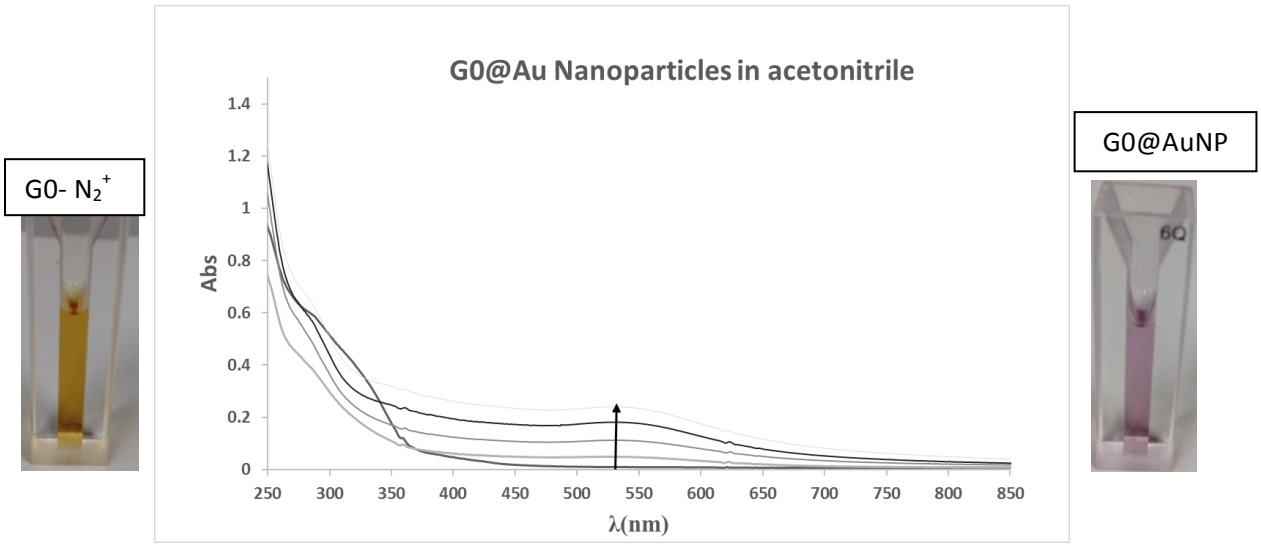

SI Figure 33. TEM images of Fresh (left/top) and Aged (right/bottom) Nanoparticles

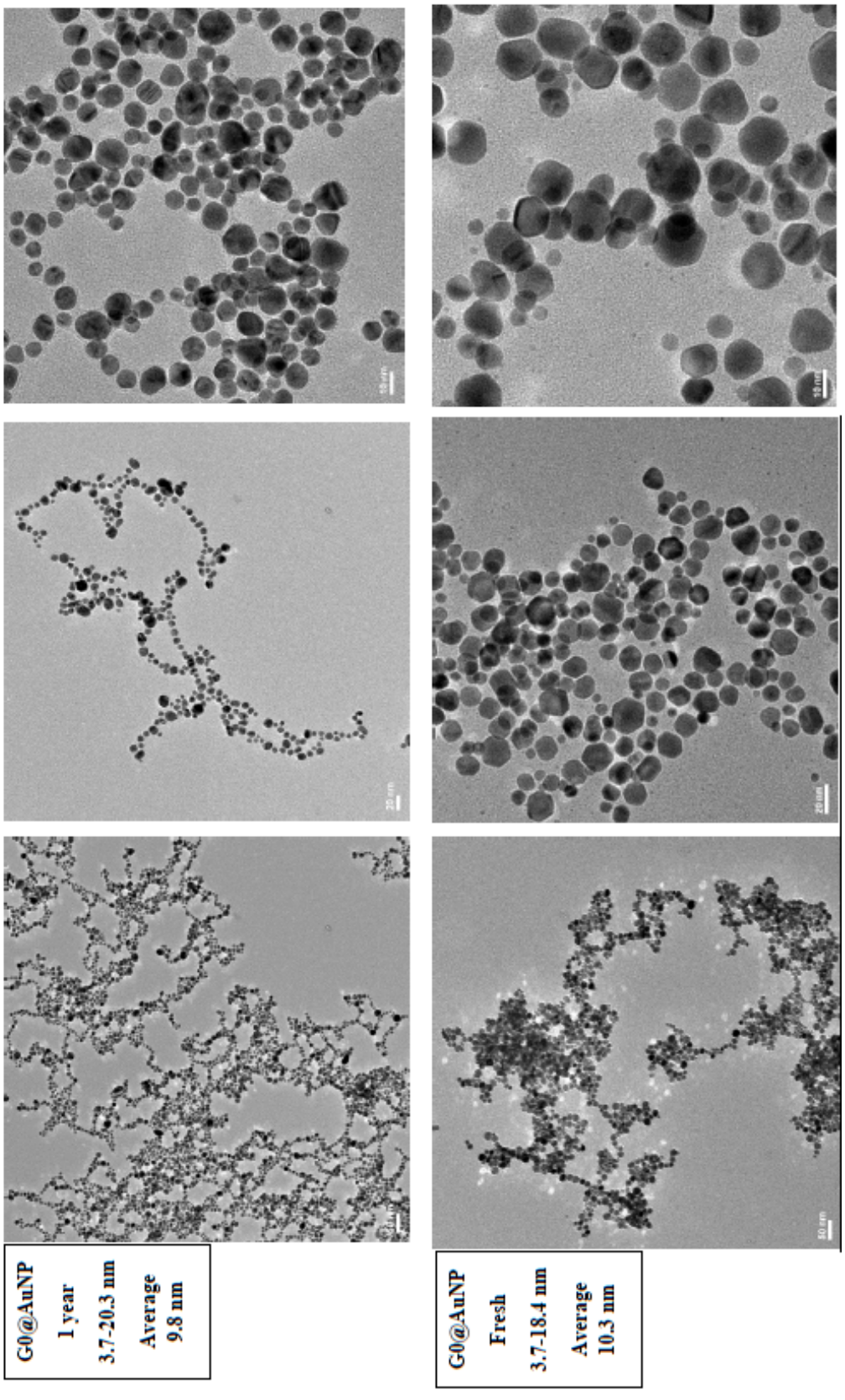

SI Figure 34. UV-vis spectra illustrating the reduction of the diazonium moiety with a solution 0.1 M of $NaBH_4$ with formation of the plasmon band at 517 nm for G1@Au NPs.

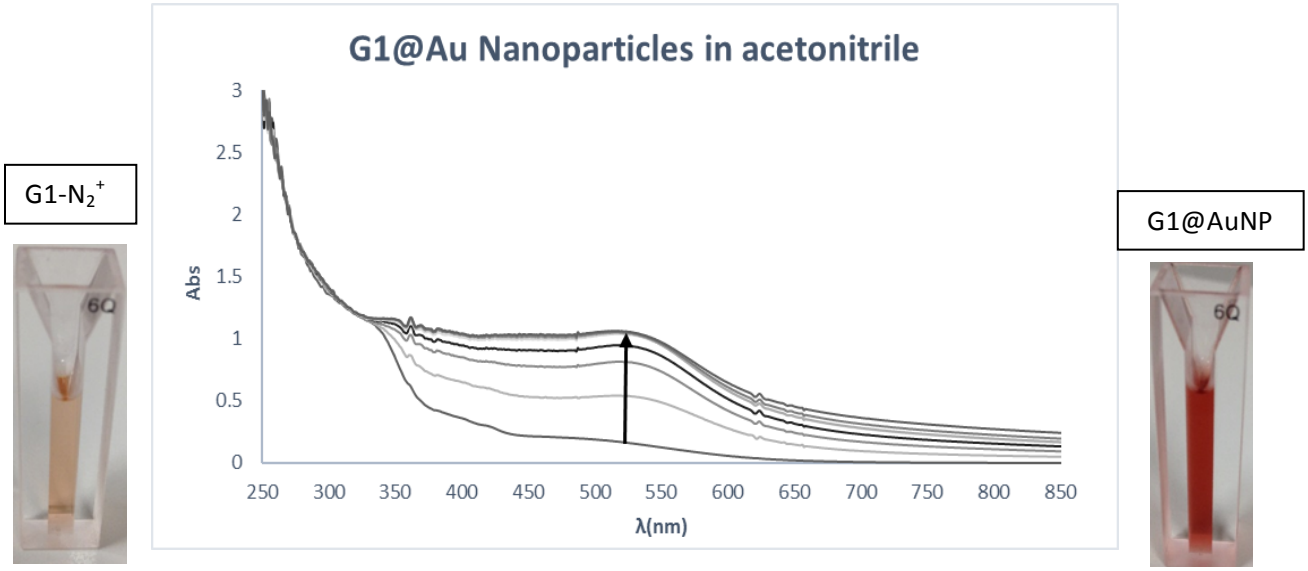

SI Figure 35. TEM images of G1@Au Fresh (left/top) and Aged (right/bottom) Nanoparticles

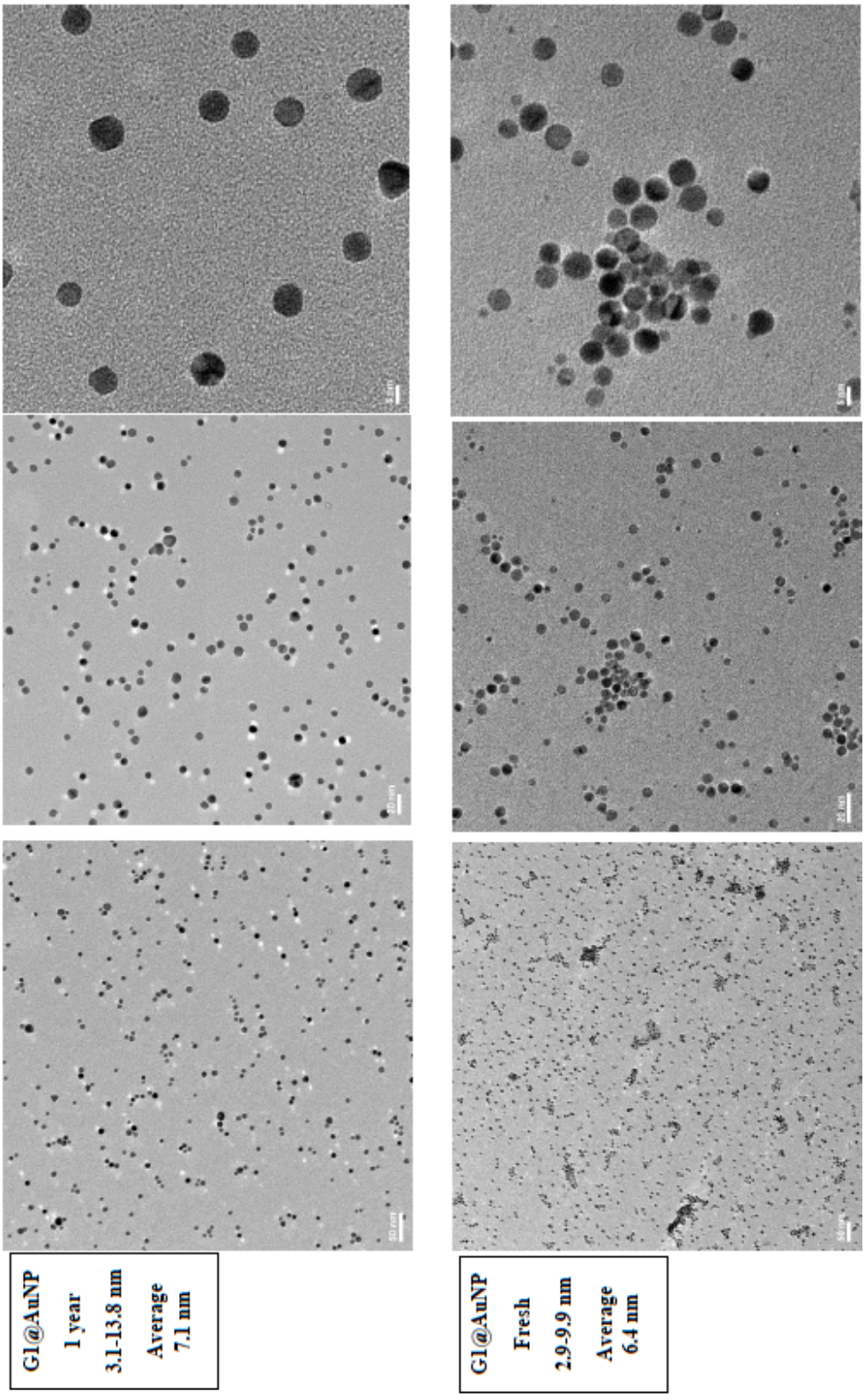

SI Figure 36. UV-vis spectra illustrating the reduction of the diazonium moiety with a solution 0.1 M of $NaBH_4$ with formation of the plasmon band at 515 nm for G2@Au NPs.

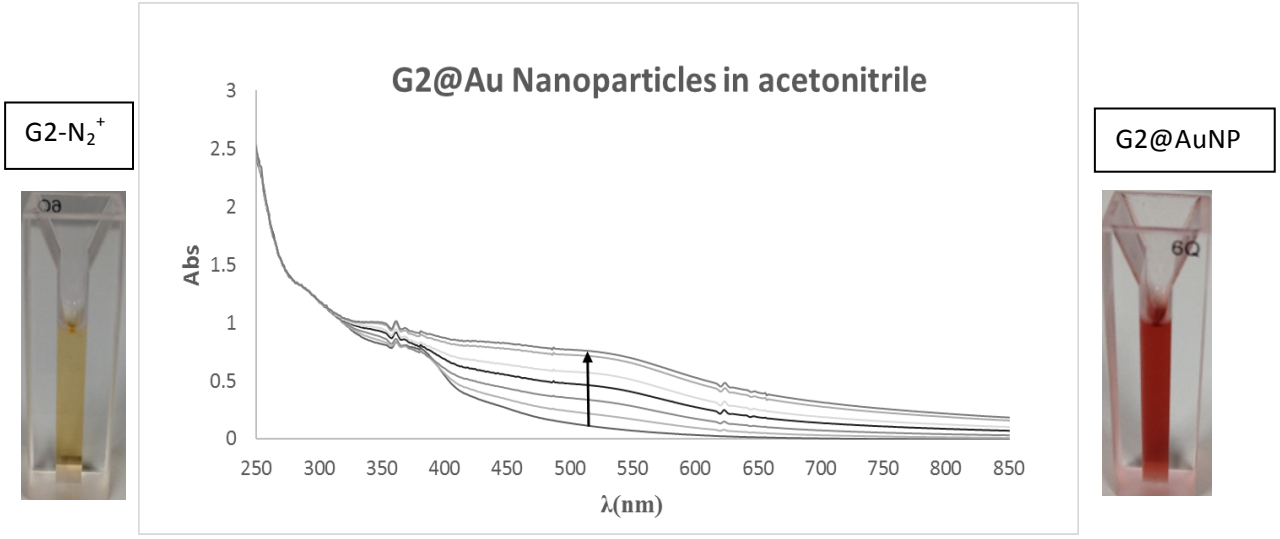

SI Figure 37. TEM images of G2@Au Fresh (top/left) and Aged (bottom/right) Nanoparticles

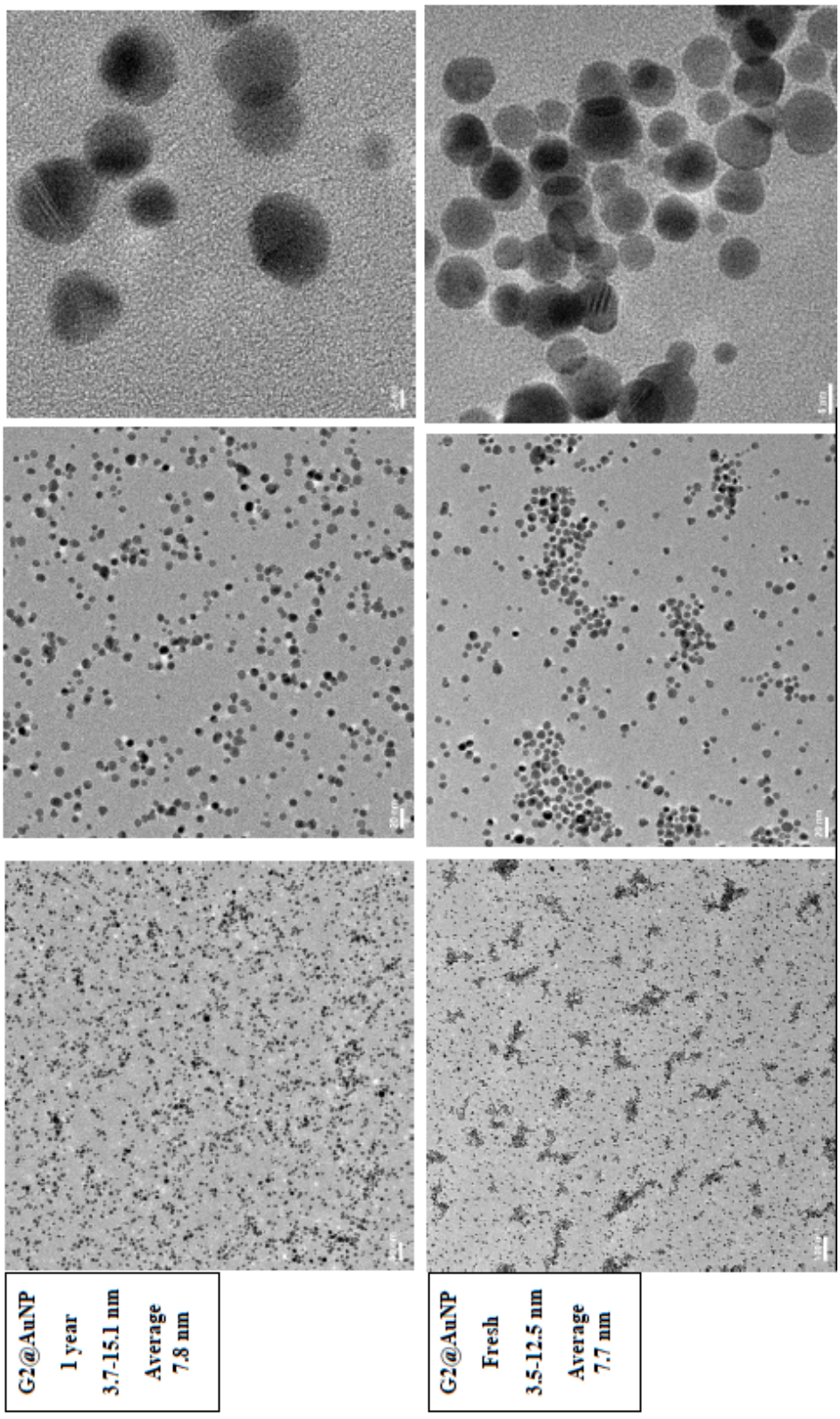

Stability Studies

The stability of the isolated dendrimers were assessed by centrifugation, sonication and heating. Absorbance at higher wavelengths is indicative of aggregation.

SI Figure 38. Stability of G0@AuNP at different conditions. Sonication and heating affect aggregate/NP size.

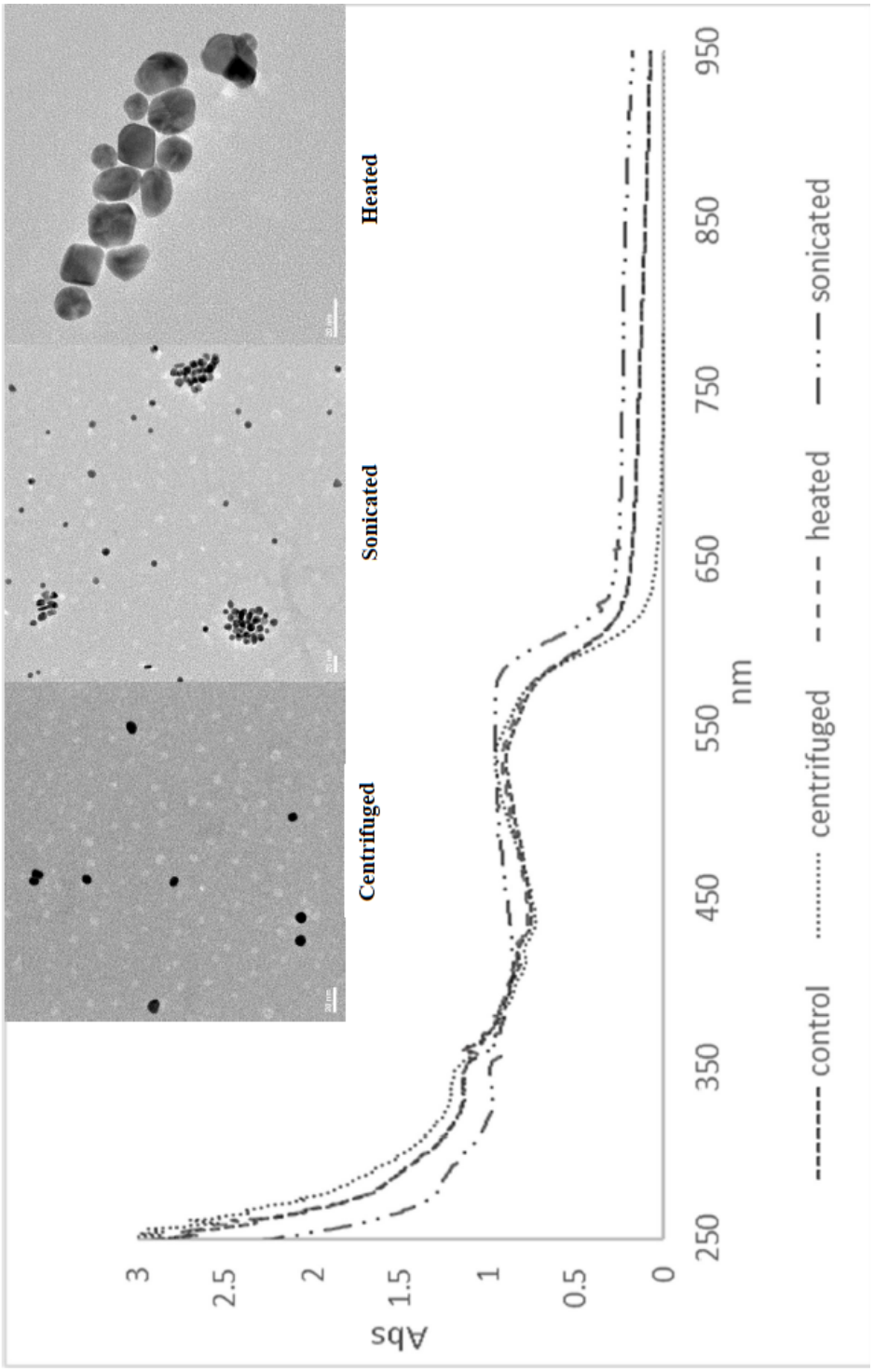

SI Figure 39. Stability of G1@AuNP at different conditions. The small change in the absorbance of G1@Au has been observed upon heating similar nanoparticles: *J. Phys. Chem. B* ***1999****, 103, 4212-4217.*

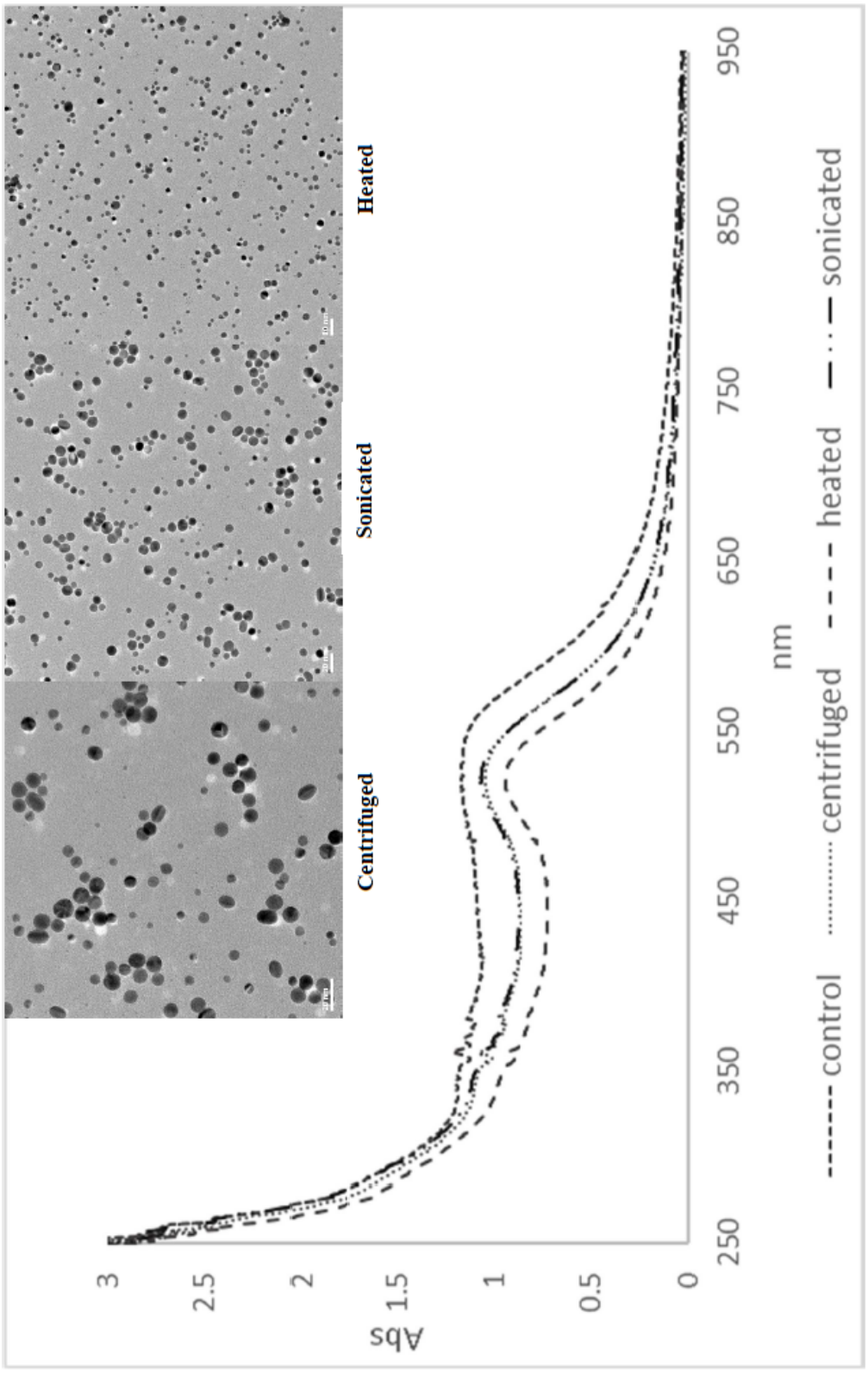

SI Figure 40. Stability of G2@AuNP at different conditions

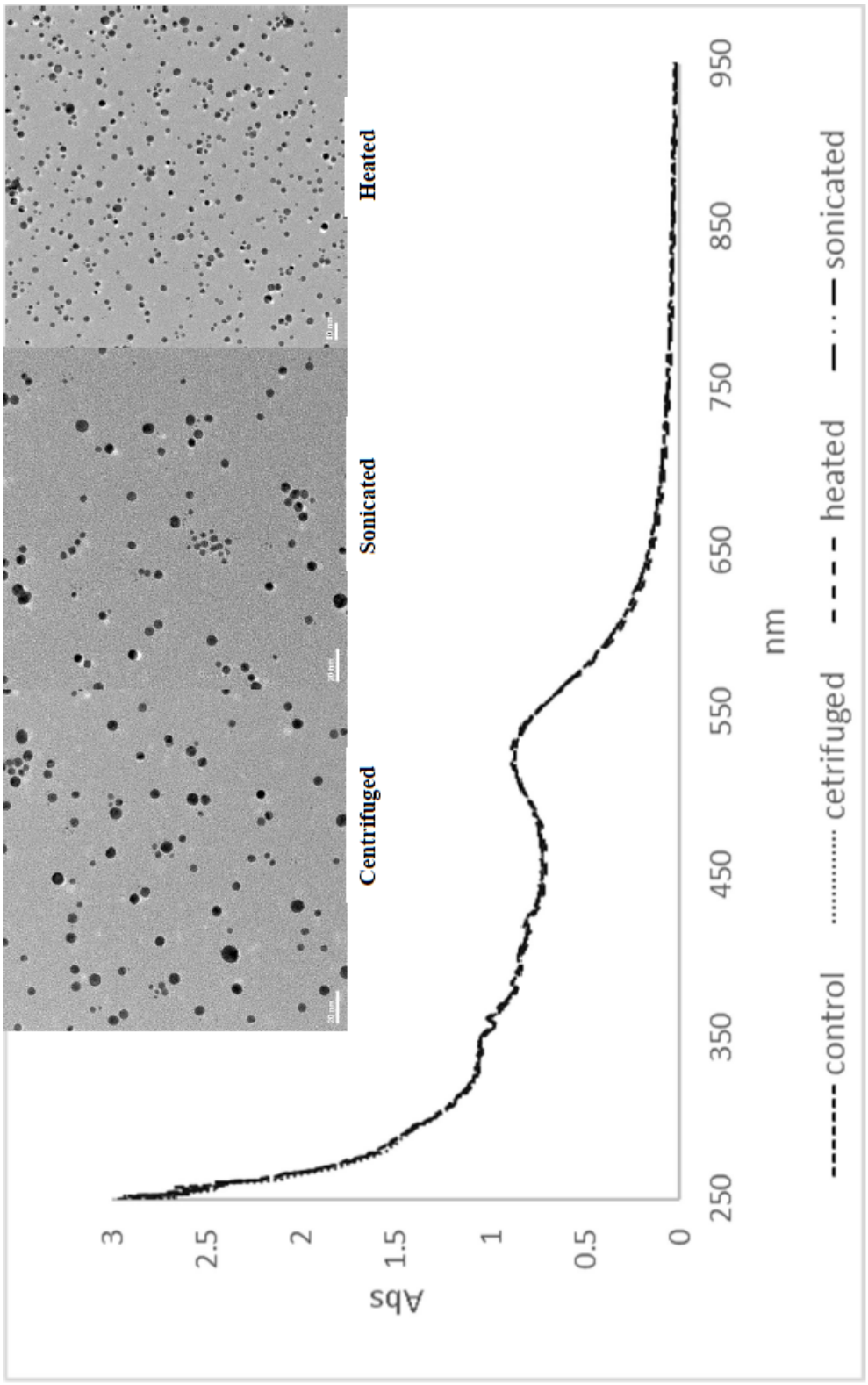

SI Figure 41. TEM images of surface coating. Arrows indicate areas where particle-particle interactions may lead to visualization of the organic coating. Alternative explanations could include particle fusion.

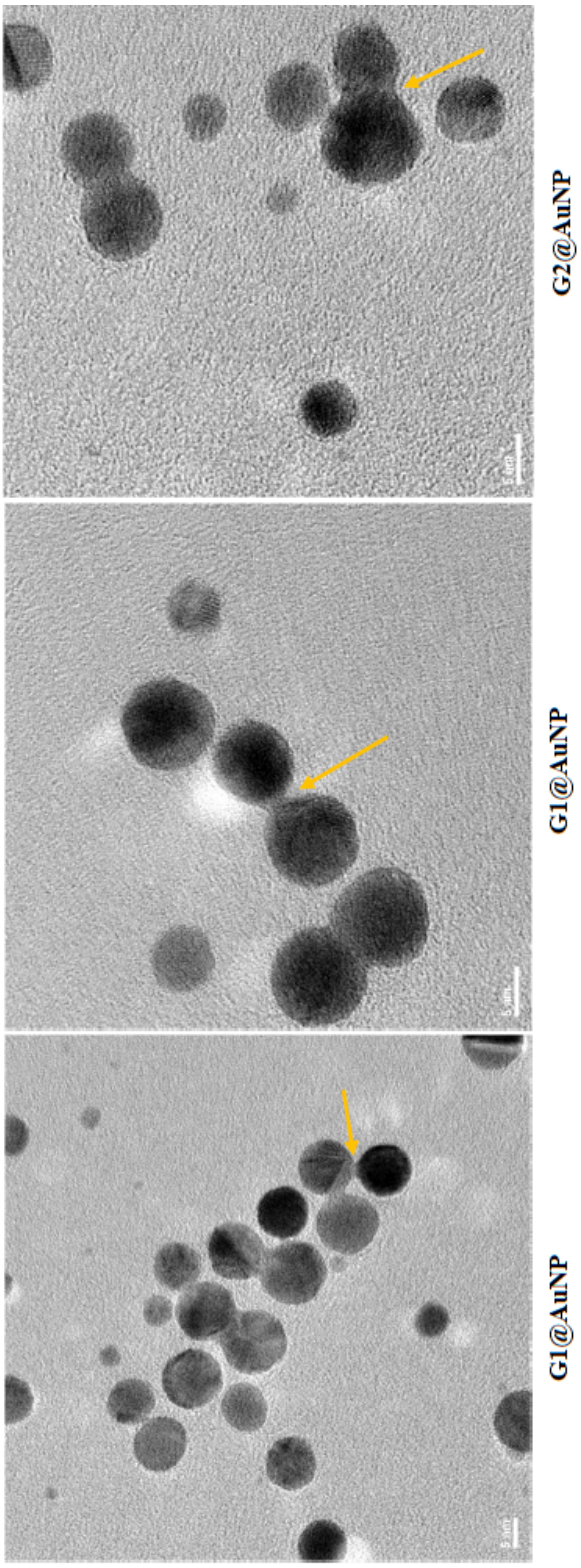

SI Figure 42 - TGA of G0@Au

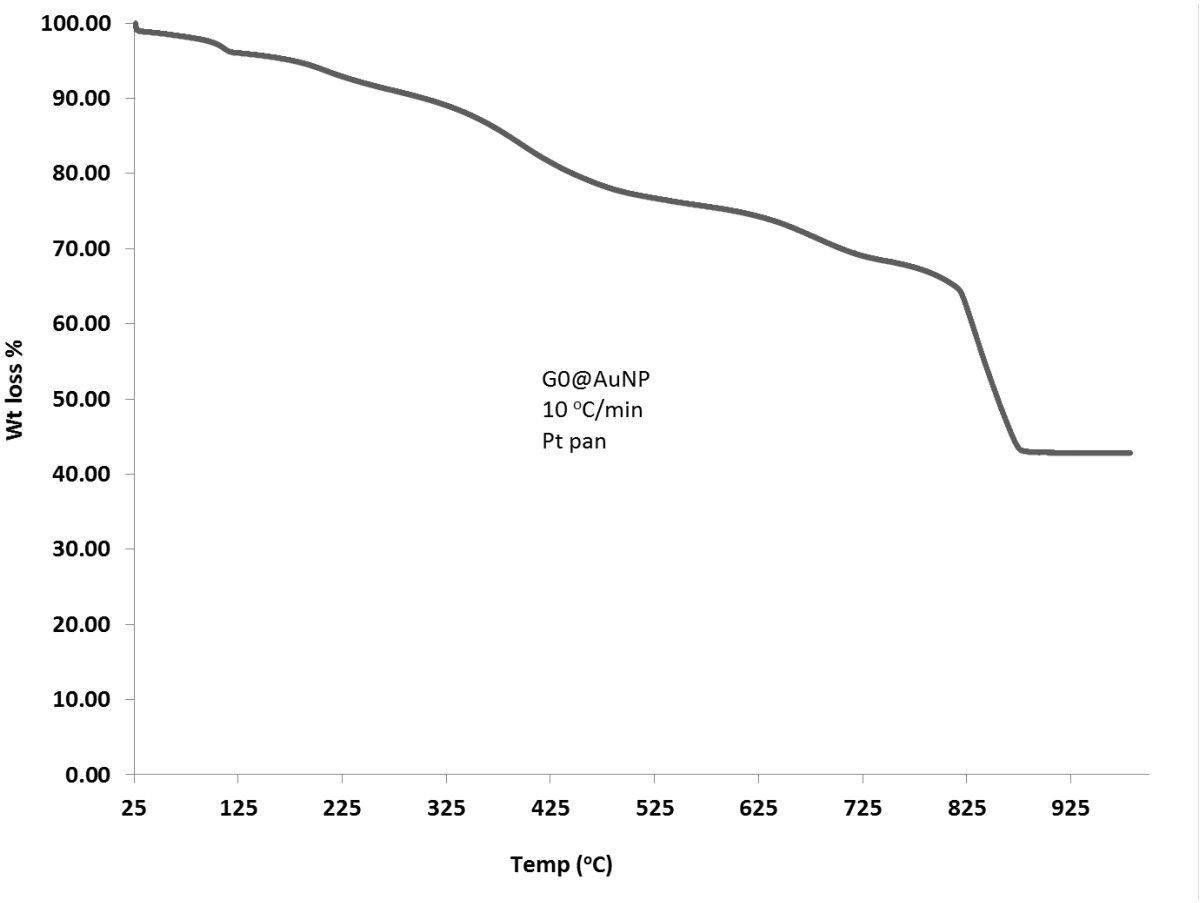

SI Figure 43 - TGA of G2@Au

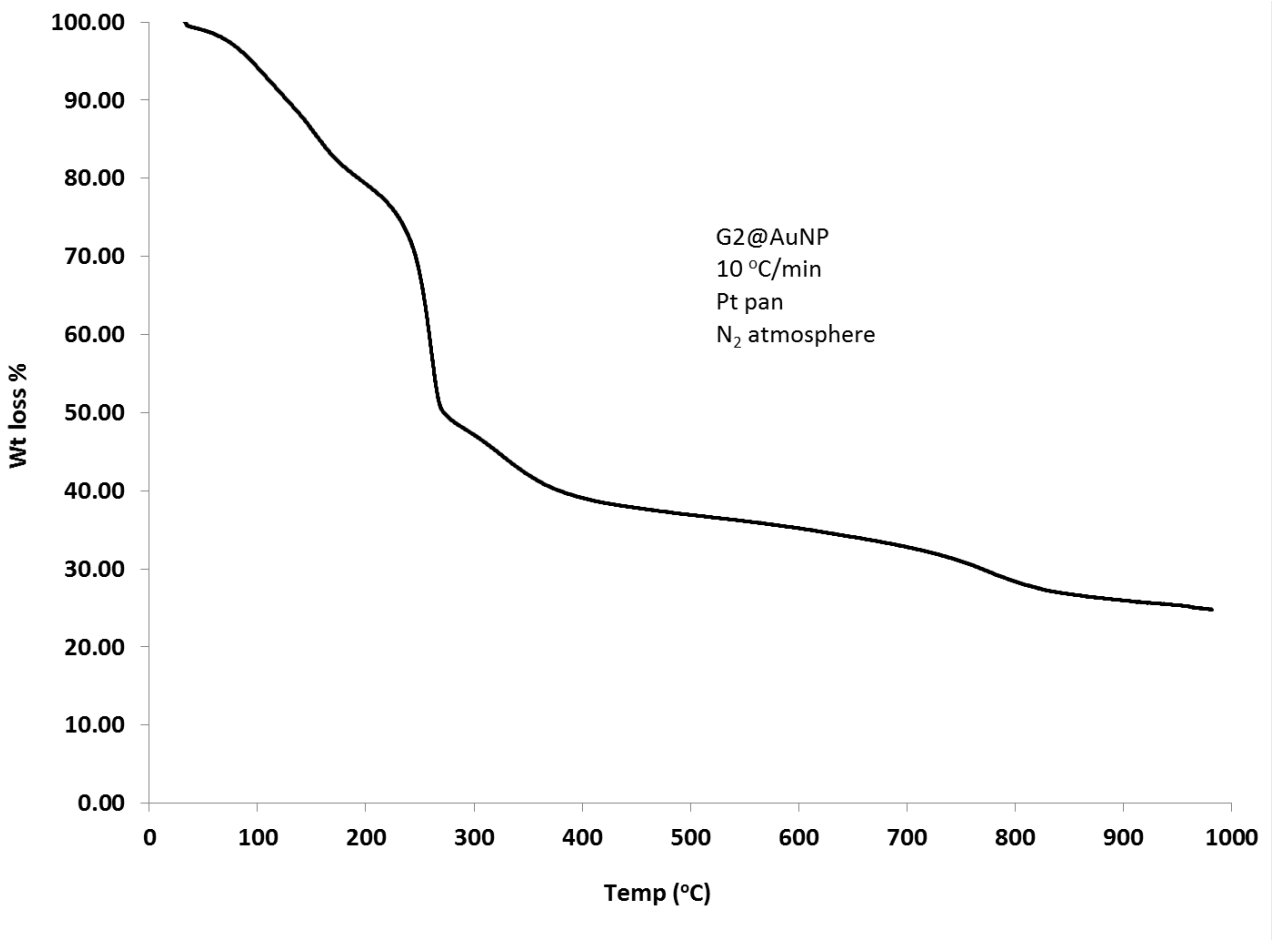

Computational details

Determination of the dendrons maximum grafting density: A first issue in the creation of the NP-dendron molecular models was to understand the expected dendron density level at the NP surface. Large excess of dendrons is present in the experiments during the formation process of the real NP-dendron systems. Thus, consistent with these experimental conditions, a maximum dendron density is expected at the surface of the NPs. To determine an appropriate value for the grafting densities of G0, G1 and G2 dendrons onto the nanoparticles, we initially aimed at understanding the maximum possible densities for the dendrons on a flat surface (planar configuration). Then, once we obtained the area per-dendon in the dense packing, we aimed at converting it onto a semisphere. Thus, we started from a reference model consisting of an array of 4x4 dendrons arranged according to a hexagonal packing (maximum density arrangement) and replicating in periodic boundary conditions generating an infinite bulk surface on the *xy* plane (Figure 44). The last carbon atoms in the dendron tails (those explicitly bound to the Au surface atoms in the NPs: see Scheme 1 in the main paper) were let free to move on the *xy* plane, while a coordinate restraint was applied in *z* direction. This setup allowed the dendron tail atoms to slide on the *xy* plane during the simulations, while being restrained in direction orthogonal to the model surface (*i.e.*, lateral relaxation of dendrons bound onto a surface).

The relaxation of three arrays for each generation of dendrons (G0, G1 and G2) was carried out in the absence of solvent (gas phase) by means of NPT molecular dynamics (MD) simulations using the GROMACS 4.5.6 simulation package.[1] This condition is consistent with the maximum achievable dendrons density on a surface – *i.e.*, the addition of water to the system

could only result in a lower density in the organic patch. These MD runs were conducted at 27 °C (300 K) of temperature and 1 atm of pressure using the v-rescale thermostat[2] and the Berendsen barostat;[3] a semi-isotropic pressure scaling was employed to allow the dendrons to optimize their lateral arrangement preserving consistency with the hexagonal packing.

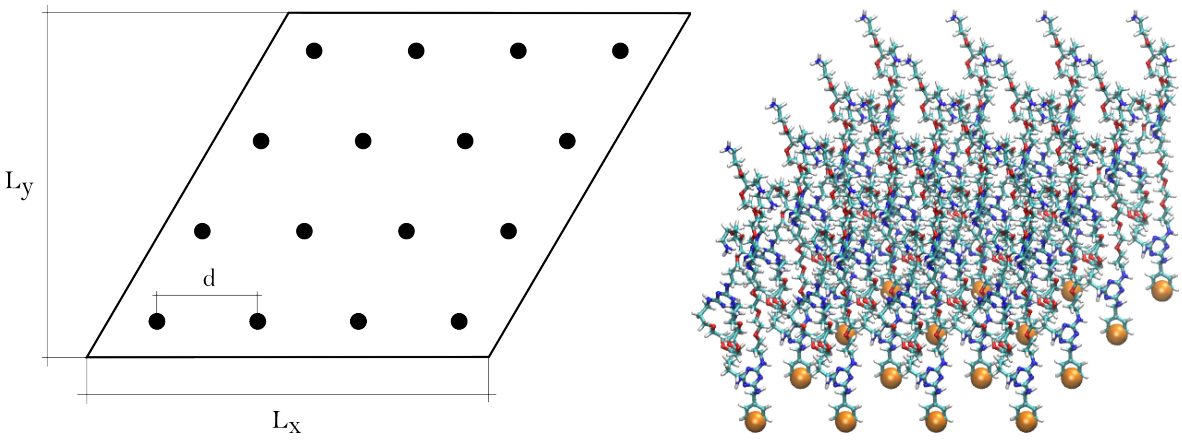

SI Figure 44. Scheme adopted to model the packing of dendrons onto a planar surface and to study the optimal dendrons spacing. The tail C atoms of the dendrons restrained in *z* direction (only sliding on the *xy* plane allowed for these atoms) are represented as orange spheres.

The box dimensions on the xy plane (Lx, Ly – see Fig. S1) were monitored over 50 ns of MD simulation, and the inter-dendron distances *d* were calculated in each case as a function of the cross sectional area of the simulation box as follows:

$$\frac{L_x L_y}{N} = d^2 \frac{\sqrt{3}}{2}$$

Where N is the number of dendrons in the box (16 in our case). The *d* spacing values (G0, G1, G2) are reported in Figure 45 as a function of simulation time. The equilibrated dendron-dendron spacing values have been used to build the nanoparticle-dendron models (see next section).

SI Figure 45 - Inter-dendrons spacing as a function of simulation time.

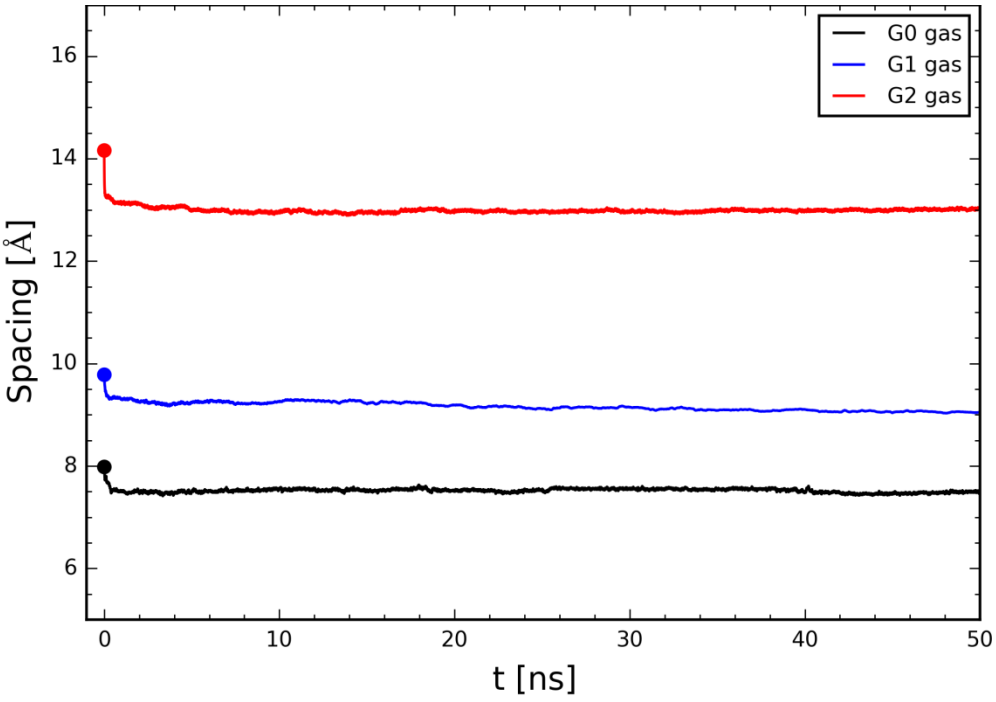

Creation and parametrization of the molecular systems: Three Au nanoparticle models (NPs) were created using the Open MD builder tool for metallic lattices.[4] The dimension of the NP models were chosen according to the average diameters observed experimentally (9.8 nm, 7.1 nm and 7.8 nm for G0@Au, G1@Au and G2@Au respectively). Given the symmetry of the systems, only half nanoparticles (half-NPs) were considered to reduce the large size of the systems to be simulated. Furthermore, since the bulk atoms of the half-NPs are not expected to interact with the adsorbates, only the first five layers of Au atoms were then considered in the

model generating a void half-NP having surface thickness of ≈10 Å (larger than the cutoff used in the simulations, see further), consistent with previous studies on Au surfaces.[5]

G0, G1 and G2 dendrons were then grafted onto the NP surfaces at a distance of 2 Å from the topmost surface Au atoms.[6] The number of dendrons for each NPs was thus determined from the surface area of the NP and the spacings as follow:

$$N_i = \frac{8\pi {R_i}^2}{3\sqrt{3}d^2}$$

where R_i is the radius of the NP and d_i the spacing of the given system.

SI Table 1. Main features of the simulated NP-dendron systems

	NP diameter[a] [nm]	Number of dendrons per half-NP	Number of waters	Total number of atoms	Box size[b] (nm)x(nm) x(nm)	Simulation time [ns]
G0@NP	9.8	300	43k	167k	16.1 x 16.1 x 11.0	20
G1@NP	7.1	156	45k	179k	15.4 x 15.4 x 9.0	20
G2@NP	7.8	56	47k	178k	15.0 x 13.0 x 10.0	30

[a]The models for the NP were constructed having the same diameter of the experimental ones. [b]To minimize the number of atoms in the system to reduce the computational burden, the simulation boxes having a rombohedric base and replicating into an hexagonal packing on the xy plane. The sides of the boxes are reported as X, Y, Z, while the angles YZ, XZ, XY are respectively 90°, 90°, 60° for all cases.

We developed an *ad hoc* iterative procedure to place the dendrons onto the NP surface. First, an uniformly sampled radial direction respect to the centre of the NP was generated; each dendron

was then aligned to that direction and translated by a displacement corresponding to the radius of the NPs augmented by the C-Au bonds length.[6] This procedure was repeated until the desired number of dendrons was inserted, allowing for a uniform distribution of dendrons onto the NP surface, and avoiding unphysical atom superpositions. Before solvation, each system was preliminary relaxed through a short minimization and MD simulation step to remove eventual bad contacts arising from the dendrons automatic placement. Explicit water molecules were used with the addition of neutralizing Cl^- ions to solvate the systems into periodic simulation boxes. Table S1 reports the main features of the NP-dendron simulated systems.

The force field parameters for the Au atoms in the NPs were taken from the literature.[7] In particular, the Au interactions with the rest of the system was modelled by a standard non-bond 12-6 Lennard Jones potential (corresponding terms: $\epsilon_0 = 5.29$ kcal/mol and $r_0 = 2.951$ Å). These parameters have already demonstrated to be consistent with a series of properties for Au fcc clusters (surface tension, elastic moduli, etc.)[7] and are well compatible with the AMBER force field[8] and with all other parameters used for the molecules present in this study. G1, G2 and G3 dendrons were created analogously to what done for previous sudies on similar molecules[9] and parametrized according the GAFF general amber force field (*gaff.dat*).[10] The TIP3P model[11] was used for the explicit water molecules present in the simulations.

Simulation procedure: The Au atoms composing the half-NP models, as well as the carbon tail atoms of the dendrons (those grafted to the Au surface), were kept fixed during all MD simulations. This setup was considered as well consitent to study the hydration level of the maximum-density organic dendron layers covering the Au nanoparticles, which is the main purpose of this modeling study.

After initial minimization, and a preliminary heating phase, G0@Au and G1@Au systems were equilibrated for 20 ns of MD simulation in NPT conditions at the temperature of 27 °C (300 K) and 1 atm of pressure. G2@Au was simulated for 30 ns, as equilibration of the larger G2 dendrons composing the organic layer in this case required a longer time. In the MD runs, a wall on the box sides perpendicular to *z* direction was applied to prevent the dendrons to fold in a unrealistic way in correspondance of the half-NP base. For all simulations, a v-rescale thermostat,[2] a Berendsen barostat[3] and a cutoff of 9 Å were used. The long range electrostatic interactions were treated with the particle mesh ewald approach,[12] and all atoms involving hydrogens were treated using the LINCS algorithm.[13] The root mean square displacement data (RMSD) were extracted from the MD trajectories and used to assess systems equilibration (Figure 46). The last 10 ns of each MD simulation were considered as representative of the equilibrated systems and used for further analysis. The radial distribution function plots of the water molecules, dendron atoms and surface charge groups in the organic layer at the NP surface (Figure 3 in the main paper) were calculated respect to the centre of the NP models (reference) and then all distances were rescaled by the NP radius (origin of the x axis in Figure 3 in the main paper coincident to the NP surface).

SI Figure 46: Root mean square displacement (RMSD) data as a function of simulation time; G0@Au and G1@Au systems were simulated for 20 ns, G2@Au system was simulated for 30 ns.

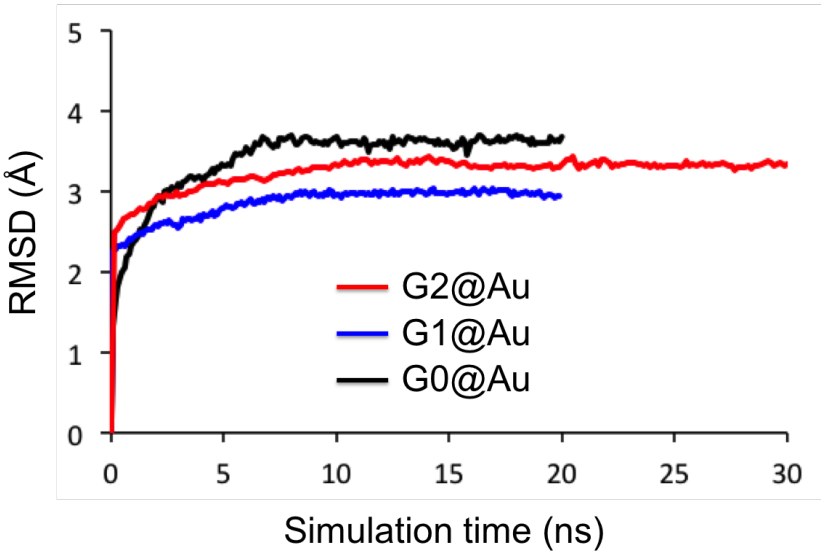

References for the Computational Models:

[1] S. Pronk, S. Pail, R. Schulz, P. Larsson, P. Bjelkmar, R. Apostolov, M. R. Shirts, J. C. Smith, P. M.; Kasson, D. van der Spoel, B. Hess, E. Lindahl, *Bioinformatics,* 2013, 29, 845-854.
[2] G. Bussi, D. Donadio, M. Parrinello, *J. Chem. Phys*. 2007, 126, 014101.
[3] H. J. C. Berendsen, J. P. M. Postma, W. F. van Gunsteren; A. Di Nola, J .R. Haak, *J. Chem. Phys*. 1984, 81, 3684-90.
[4] J. Michalka, J. Marr, K. Stocker, M. Lamichhane, P. Louden, T. Lin, C. F. Vardeman II, C. J. Fennell, S. Kuang, X. Sun, C. Li, K. Daily, Y. Zheng, M. A. Meineke, J. Daniel, *University of Notre Dame: Notre Dame, IN*, 2010.
[9] G. Doni, M. Nkoua-Ngavouka, A. Barducci, P. Parisse, A. De Vita, G. Scoles, L. Casalis, G. M. Pavan, *Nanoscale* 2013, 5, 9988-9993.
[6] D. Benitez, N. D. Shapiro, E. Tkatchouk, Y. Wang, W. A. Goddard III, F. F. Toste, *Nature Chem.* 2009, 1, 482-486.
[7] H. Heinz, R. A. Vaia, B. L. Farmer, R. R. Naik, *J. Phys. Chem. C*, 2008, 112 (44), 17281–17290.
[8] D. A. Case, T. E. Cheatham, T. Darden, H. Gohlke, R. Luo, K. M. Merz, A. Onufriev, C. Simmerling, B. Wang, R. J. Woods, *J. Comput. Chem.* 2005, 26, 1668–1688.
[9] (a) D. A. Torres, M. Garzoni, A. V. Subrahmanyam, G. M. Pavan, S. Thayumanavan, *J. Am. Chem. Soc.* 2014, 136, 5385-5399; (b) M. Garzoni, K. Okuro, N. Ishii, T. Aida, G. M. Pavan. *ACS Nano* 2014, 8, 904-914; (c) M. Garzoni, N. Cheval, A. Fahmi, A. Danani, G. M. Pavan, *J.*

Am. Chem. Soc. 2012, 134, 3349-3357; (d) G. M. Pavan, A. Danani, S. Pricl, D. K. Smith, *J. Am. Chem. Soc.* 2009, 131, 9686-9694.
[10] J. Wang, R. M. Wolf, J. W. Caldwell, P. A. Kollman, D. A., Case, *J. Comput. Chem.*, 2004, 25(9):1157-74.
[11] W. L. Jorgensen, J. Chandrasekhar, J. D. Madura, R. W. Impey, M. L. Klein, *J. Chem. Phys.,* 1983, 79, 926. [12] T. Darden, D. York, L. Pedersen, *J. Chem. Phys.*, 1993, 98, 10089.
[13] B. Hess, H. Bekker, H. J. C. Berendsen, J. G. E. M. Fraaije, *J. Comp. Chem.* 1997, 18 (12): 1463–1472.

General Experimental for XPS and SIMS Analysis

X-ray Photoelectron Spectroscopy (XPS). Photoelectron spectra were measured using a PHI 5000 VersaProbe Scanning ESCA Microprobe (Physical Electronics, Chanhassen MN) equipped with a monochromatic Al Kα X-ray source (E_p = 1486.7 eV). Typically the pressure was <7 x 10^{-10} mbar during analysis. The XPS spectra were measured with a pass energy of 23.5 eV and energy step 0.125 eV. The data were collected at 45 º to the normal of the sample surface, and were calibrated using the C1s photoelectron peak (E_B = 285.00 eV). The data were analyzed using Spectra were analyzed using CasaXPS 2.3.16 (RBD Instruments, Inc., Bend, OR) and AAnalyzer 1.07.

Time-of-Flight Secondary Ion Mass Spectrometry (TOF SIMS). Time-of-flight secondary ion mass spectra were acquired using an ION TOF IV spectrometer (ION TOF Inc, Chestnut Hill NY) equipped with a Bi liquid metal ion gun. Briefly, the instrument consists of three vacuum chambers which are separated by a gate valves. The samples are introduced via a loadlock. The preparation and analysis chambers are maintained at ≤7 x 10^{-9} mbar. The primary Bi^+ ions had a kinetic energy of 25 keV, contained with an ~100 nm diameter probe beam and rastered over a (500 × 500) μm^2 area. All spectra were obtained in the static regime using a total ion dose of less than 10^{10} ions cm^{-2}. The secondary ions were extracted into a time-of-flight mass spectrometer using a potential of 2kV and reaccelerated to a kinetic energy of 10 keV before arriving at the detector. For each sample at least three areas were examined, and the spectra reported are representative of the data obtained.

SI Figure 47. Au 4f, C 1s, O 1s, F 1s and N 1s photoelectron spectra of G0@Au. Also shown is the fit to the data.

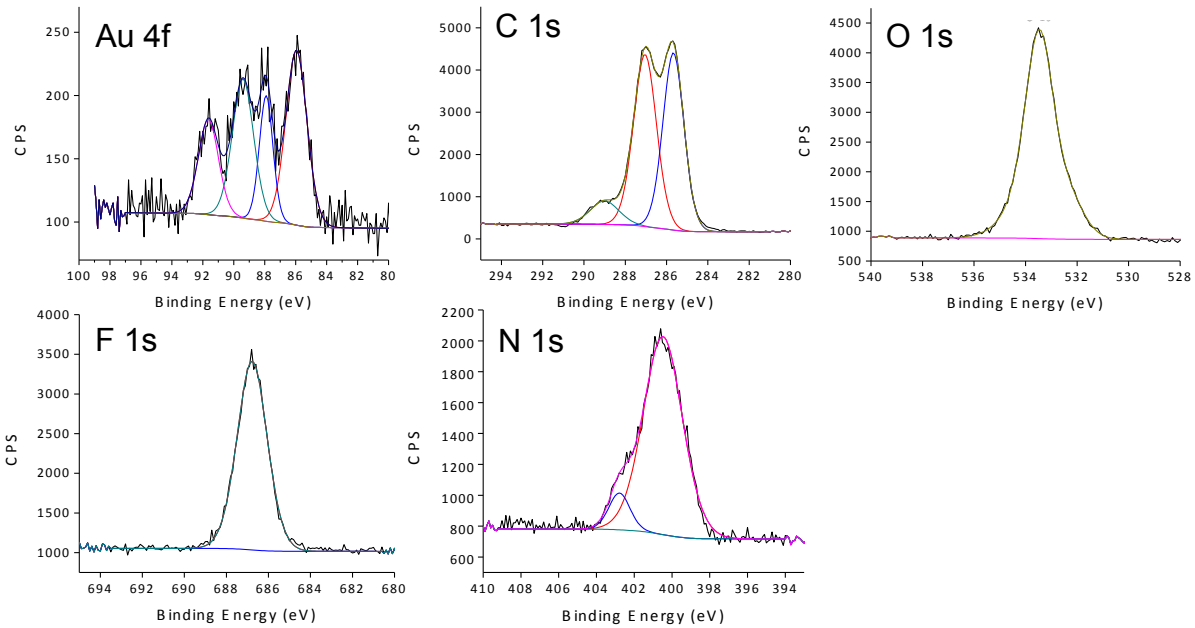

The XPS spectra show marked changes in the elemental compositions of the dendron-coated gold nanoparticles. The analysis of the G0@Au samples shows that there are 5 elements present: Au, C, O, N, F (Figure 47). In the Au 4f spectra, four peaks are observed. The doublet at 84 eV ($4f_{7/2}$) and 88 eV ($4f_{5/2}$) indicates that there is some Au present as Au(0), the metallic element. The doublet at 89.4 eV ($4f_{7/2}$) and 91.6 eV ($4f_{5/2}$) indicates that some Au is present in a higher oxidation state, and suggests that there are Au-F bonds present. A single F 1s peaks is observed with a binding energy (E_B) of 687 eV and is attributed to the interaction of $[NO]PF_6$ with Au. Taken together, the data indicate that the reaction is not fully complete, and may account for the wide distribution of nanoparticle size. Three photoelectron peaks – N 1s, C 1s and O 1s – are indicative of the presence of the G0 dendrimer. In the N 1s spectrum two photoelectron peaks are observed at 400 eV and 403 eV which are assigned to $–C\underline{N}H_2$ and N present in organic polymers, such as $–C(CH_3)_2C(CH_3)2\underline{N}(O)\underline{N}(O)$. Three different carbons are present $\underline{C}$-H or $\underline{C}$-$\underline{C}$ (E_B = 285 eV), $\underline{C}$-O (E_B = 287 eV) and $–\underline{C}OO$ (E_B = 289 eV). The O1s peak is broad with a maximum at 533.5 eV and cannot be easily deconvolved, but is consistent with oxygen present in polymers.

SI Figure 48. Au 4f, C 1s and O1s photoelectron spectra of G1@Au. Also shown is the fit to the data.

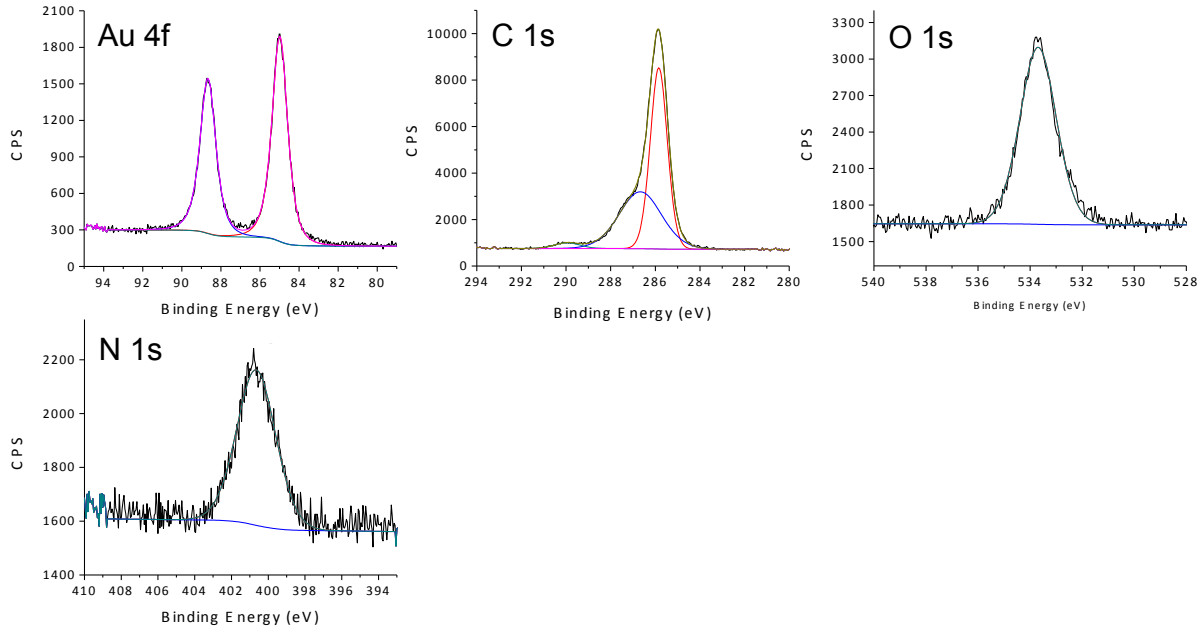

For the G1@Au samples, the photoelectron spectra show one type of Au is present as Au(0) indicating that the reaction is complete (Figure 48). Further no F is observed. The presence of the dendrimer is indicated by 3 photoelectron peaks, N 1s, C1s and O1s. The C1s region can be deconvolved into 3 contributions which are assigned to C-H or C-C (E_B = 285 eV), C-O (E_B = 287 eV) and –COO (E_B = 289 eV). We note that there is an increase in the relative amounts of C-O species present and a decrease in the concentration of –COO (Figure S2). In the N 1s spectrum there is single peak at a binding energy of 400.8 eV, which is indicative of CNO species. The O1s peak is broad with a maximum at 533.7 eV and is consistent with oxygen present in the dendrimer shell.

SI Figure 49. C 1s and O1s photoelectron spectra of G2@Au. Also shown is the fit to the data.

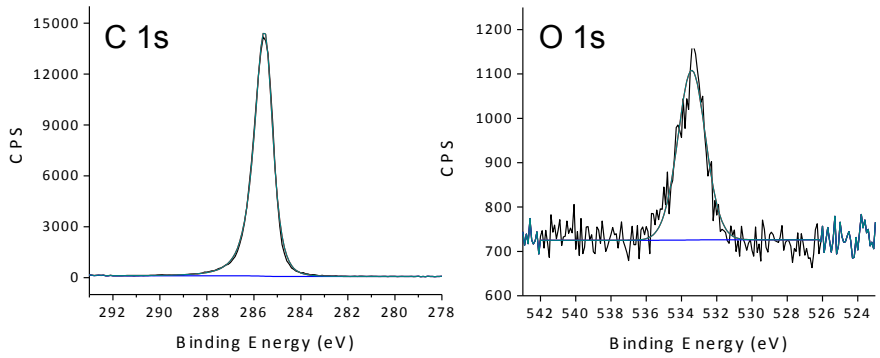

In the XPS photoelectron spectrum for G2@Au only C 1s and O 1s photoelectron peaks are observed (Figure 49), which is consistent with the dendrimer shell increasing in thickness. A single photoelectron peak is observed in the C 1s peak at 285 eV (C-H or C-C). The O1s peak is broad with a maximum at 533.4 eV and is consistent with oxygen present in polymers.

SI Figure 50. Positive (a,b) and negative ion (c,d) mass spectra of G0@Au.

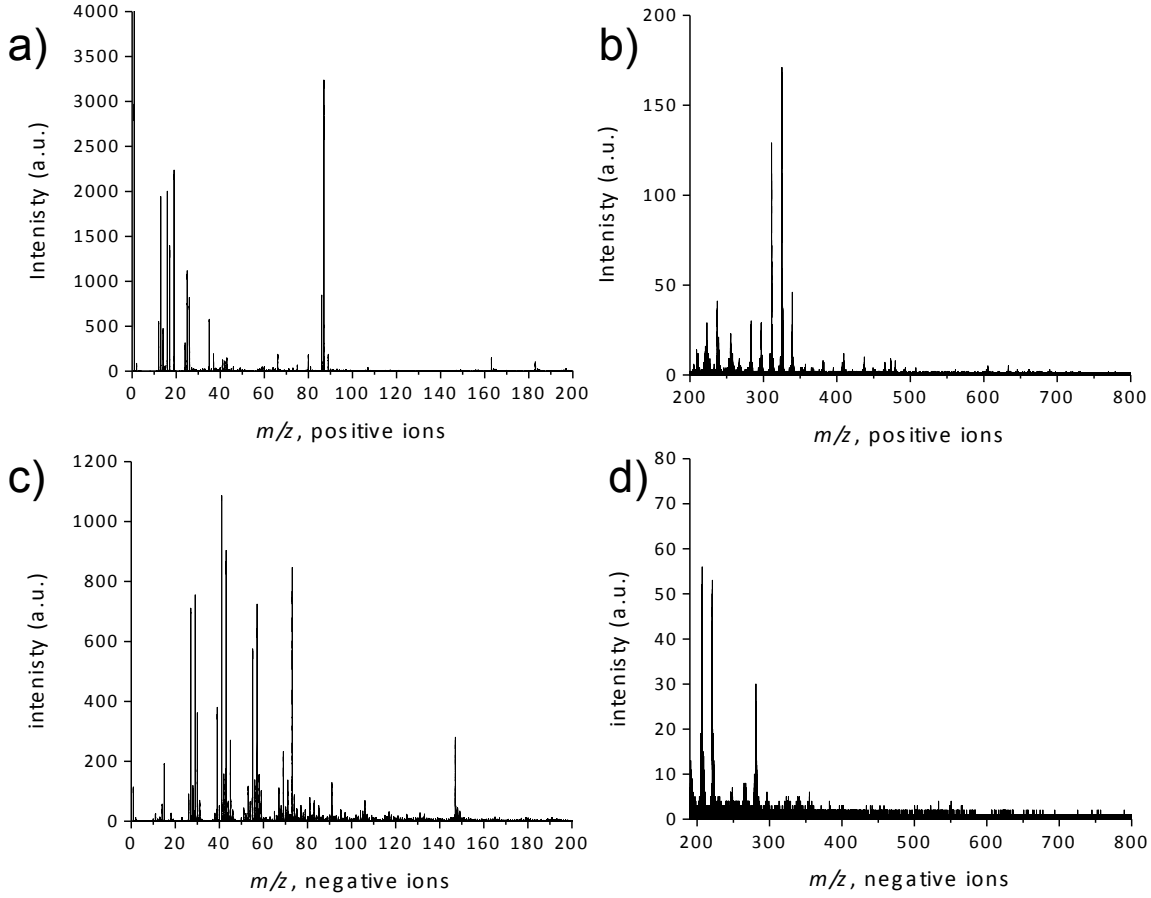

The TOF SIMS data also show significant changes with increasing dendrimer shell thickness. The G0@Au nanoparticles are the only sample where the interaction of the Au with the dendrimer is observed. In mass spectra we observe $Au^{\pm}$ ions indicative of the underlying Au nanoparticle. In the positive ion mass spectrum we also observe ions of the form $Au(CH)_n^+$ (e.g. *m/z* 223, 237) and $Au(CH_2)_xO^+$ (e.g. *m/z* 283, 297, 311, 325, 339) which suggests that Au-C bonds are present (Figure 50b). We also observe ions of the form $(CH_2)_xCH_3^+$, $(CH_2)_x^+$, $(CH_2)_x(CH)_y^+$ (e.g. *m/z* 281) and $C_xH_yO_z^+$ (*m/z* 87) (Figure 50 a,b). In the negative ion spectrum we observe ions of the form $C_xH_yO_z^-$ (e.g. *m/z* 207, 221, 281) as well as ions characteristic of hydrocarbons (Figure 50 c,d). These ions are all consistent with the formation of dendrimer. We note that in the negative ion spectra F^- (*m/z* 19) ions are observed in agreement with the XPS data and confirm that for G0@Au nanoparticles the reaction is incomplete.

SI Figure 51. Positive (a,b) and negative ion (c,d) mass spectra of G1@Au.

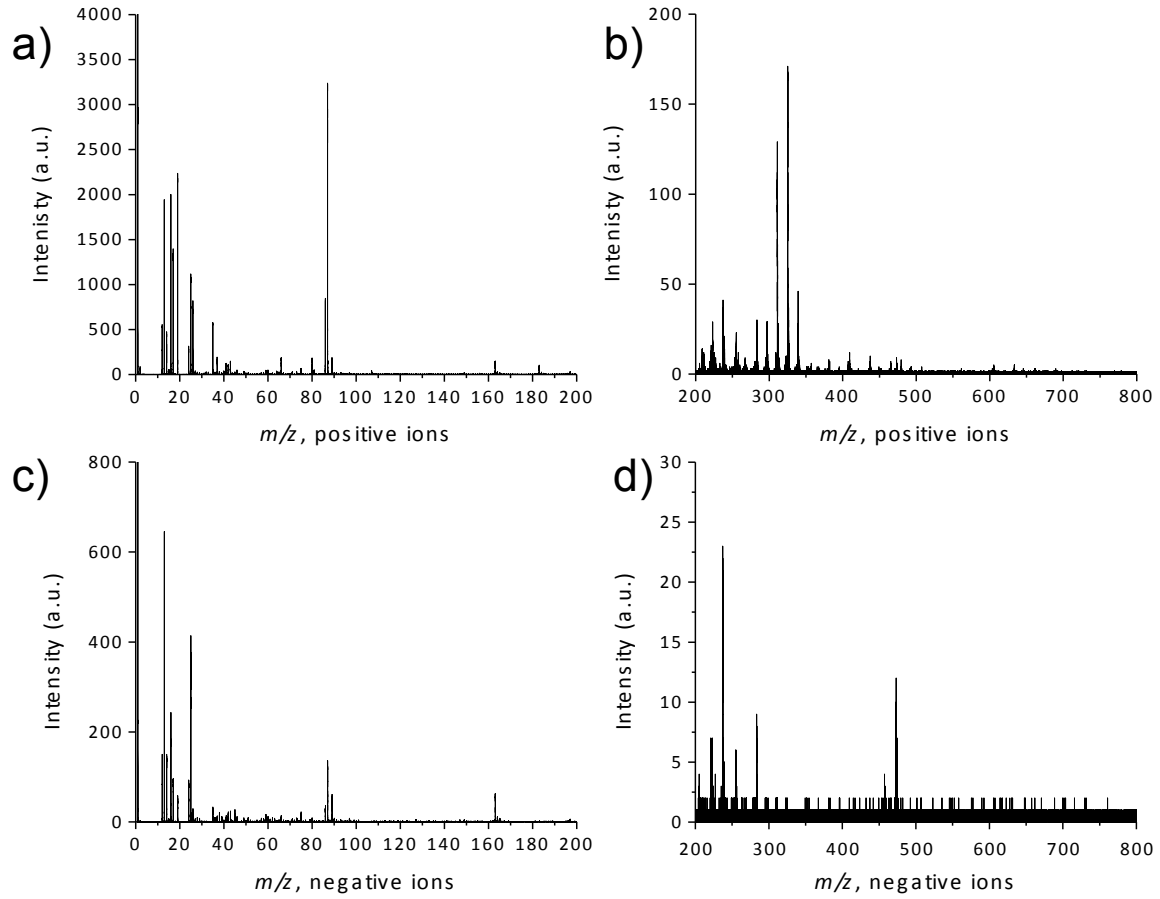

The G1@Au (Figure 51) and G2@Au (Figure 52) nanoparticles have similar mass spectra. No $Au^{\pm}$ ions are observed indicating that the dendrimer shell thickness has increased. In the positive ion mass spectra we observe ions of the form $(CH_2)_nCH_3^+$, $(CH_2)_n^+$, $(CH_2)_n(CH)_y^+$ (*m/z* 221, 281) and $C_xH_yO^+$ (*m/z* 281, 647, 662). In the negative ion spectra we observe ions of the form $C_xH_yO^-$ (*m/z* 207, 221, 281, 473). Taken together the observation of larger *m/z* ions and the characteristic form of the ions indicates that the dendrimers are becoming longer which is consistent with an increased shell thickness. We also note that as the shell thickness increases the ion intensities of the higher *m/z* also increases; for example in the negative ion spectra, the ion at *m/z* 473 has a significantly larger intensity for the G2@Au samples than for G1@Au.

SI Figure 52. Positive (a,b) and negative ion (c,d) mass spectra of G2@Au.